Research Square

Preprints are preliminary reports that have not undergone peer review.
They should not be considered conclusive, used to inform clinical practice,
or referenced by the media as validated information.

Increased Association of Deamidated αA-$_{N101D}$ with Lens Membrane of Transgenic αA$_{N101D}$ vs. Wild Type αA Mice: Potential Effects on Intracellular Ionic Imbalance and Membrane Disorganization

Om Srivastava (srivasta@uab.edu)
Birmingham City University Kenrick Library https://orcid.org/0000-0001-5727-4801
Kiran Srivastava
University of Alabama at Birmingham
Roy Joseph
University of Alabama at Birmingham
Landon Wilson
University of Alabama at Birmingham

Research article

Keywords: Lens, Crystallins, Deamidation, Post-translational modifications, Transgenic Mice, Cataract

Posted Date: November 20th, 2020

DOI: https://doi.org/10.21203/rs.2.17769/v5

License: This work is licensed under a Creative Commons Attribution 4.0 International License.
Read Full License

Version of Record: A version of this preprint was published at BMC Ophthalmology on December 10th, 2020. See the published version at https://doi.org/10.1186/s12886-020-01734-0.

Abstract

We have generated two mouse models, in one by inserting the human lens αAN101D transgene in CRYαA$_{N101D}$ mice, and in the other by inserting human wild-type αA-transgene in CRYαA$_{WT}$ mice. The CRYαA$_{N101D}$ mice developed cortical cataract at about 7-months of age relative to CRYαA$_{WT}$ mice. The objective of the study was to determine the following relative changes in the lenses of CRYαA$_{N101D}$- vs. CRYαA$_{WT}$ mice: age-related changes with specific emphasis on protein insolubilization, relative membrane-association of αA$_{N101D}$ vs. WTαA proteins, and changes in intracellular ionic imbalance and membrane organization.

Methods: Lenses of varying ages from CRYαA$_{WT}$ and CRYαA$_{N101D}$ mice were compared for an age-related protein insolubilization. The relative lens membrane-association of the αAN101D- and WTαA proteins in the two types of mice was determined by immunohistochemical-, immunogold-labeling-, and western blot analyses. The relative levels of membrane-binding of recombinant αA$_{N101D}$- and WTαA proteins was determined by an *in vitro* assay, and the levels of intracellular Ca^{2+} uptake and Na, K-ATPase mRNA were determined in the cultured epithelial cells from lenses of the two types of mice.

Results: Compared to the lenses of CRYαA$_{WT}$, the lenses of CRYαA$_{N101D}$ mice exhibited: (A) An increase in age-related protein insolubilization beginning at about 4-months of age. (B) A greater lens membrane-association of αAN101D- relative to WTαA protein during immunogold-labeling- and western blot analyses, including relatively a greater membrane swelling in the CRYαA$_{N101D}$ lenses. (C) During *in vitro* assay, the greater levels of binding αAN101D- relative to WTαA protein to membranes was observed. (D) The 75% lower level of Na, K-ATPase mRNA but 1.5X greater Ca^{2+} uptake were observed in cultured lens epithelial cells of CRYαA$_{N101D-}$ than those of CRYαA$_{WT}$ mice.

Conclusions: The results show that an increased lens membrane association of αA$_{N101D}$-relative WTαA protein in CRYαA$_{N101D}$ mice than CRYαA$_{WT}$ mice occurs, which causes intracellular ionic imbalance, and in turn, membrane swelling that potentially leads to cortical opacity.

Background

Although the cornea is the primary refractive tissue performing 70-80% of refraction of the eye, the major function of the lens is in accommodation and to partly help in the refraction. The lens accommodative function gradually diminishes with age, and is almost completely lost at age of > 50 years. The lens transparency plays an important role in focusing light on to the retina, but this role is gradually lost as it develops age-related opacity. Several unique factors maintain lens transparency for up to > 60 year of our life time. These include: cellular homeostasis among only two types of cells (epithelial and fiber cells) [1], an orderly terminal differentiation of epithelial to fiber cells with precise organelles loss [2], the unique interactions among crystallins [3], with almost no protein turnover [4], the specialized lens metabolism [5], specific interactions among α-crystallin and membrane [6], the precise maintenance of intracellular and

extracellular ionic concentrations [7], the low levels of cellular water and oxygen in the lens inner cortex and nuclear regions [8], and a unique membrane lipid composition [9]. Alterations among some of these lens unique factors play direct or indirect roles in pathogenesis of cataracts (e.g., pediatric- and age-related cataracts). However, additional cataract-causative factors are also identified, which include mutations in crystallins [10], oxidative insults of crystallins, the loss of redox balance of glutathione [11], extensive truncations of α-, β-, and γ-crystallins [12-20], a variety of post-translational modifications with deamidation as being the most abundant [21-25], and the loss of membrane integrity [7, 26, 27]. These factors individually or in combination also cause lens opacity through altered lens cellular structures and contents, ionic imbalance, increased water and oxygen levels, loss of natural interactions among crystallins, and crystallins' unfolding, degradation and cross-linking.

Our focus in this study is the potential roles of deamidation of Asn_{101} of αA crystallin to Asp that introduces negative charges and shown to alter their hydrophobicity, tertiary structures, crystallin-crystallin interactions, and leads to aggregation and cross-linking [21-27]. In this study, the deamidation of Asn_{101} to Asp in in a mouse model was studied to determine phenotypic and molecular changes within the lens due to deamidation of a single nucleotide change in CRYAA crystallin gene. This site was chosen because our past study showed that only deamidation of Asn localized at specific sites in crystallins (e.g., deamidation of N101 but not of N123 residues in αA-crystallin [24], and of N146 but not of N78 of αB-crystallin) exhibited the above-described deamidation-induced effects [25]. To show the potential effects of deamidation *in vivo*, we have generated mouse models by inserting the human lens αA-N101D transgene in CRYαA$_{N101D}$ mice, and human lens wild-type αA-transgene in CRYαA$_{WT}$ mice (to act as a control). The CRYαA$_{N101D}$ mice developed cortical cataract at about 7-months of age relative to CRYαA$_{WT}$ mice [28, 29]. This model showed for the first time that *in vivo expression* of the deamidated αAN101D caused cortical lens opacity, which was due to the disruption of fiber cell structural integrity and protein insolubilization as aggregation [28]. The comparative RNA sequencing and Ingenuity Pathway Analyses (IPA) of lenses from 2- and 4-months old CRYαA$_{N101D}$- and CRYαA$_{WT}$ mice showed that the genes belonging to cellular assembly and organization, cell cycle and apoptosis networks were altered in αA$_{N101D}$ lenses [29]. This was accompanied with several cellular defects in αA$_{N101D}$ lenses that included defective terminal differentiation (increased proliferation and decreased differentiation) of epithelial cells to fiber cells, and reduced fiber cells denucleation and expressions of Rho A and Na, K-ATPase (the major lens membrane-bound molecular transporter) [29]. The findings also suggested the potential role of lens intracellular ionic imbalance as the major reason for the development of cataract [29]. The above findings suggested that the altered intracellular ionic imbalance could be due to potential loss of membrane integrity that caused cortical opacity at about 7-months of age in the CRYαA$_{N101D}$ mouse model. Therefore, the focus of the present study was to determine whether an increased membrane-association of αA$_{N101D}$ potentially compromises membrane integrity, and causes an ionic imbalance and leads to cataract development.

Methods

Ethics Statement

All animal experiments were performed per protocols approved by the Institutional Animal Care and Use Committee (IACUC) of the University of Alabama at Birmingham (Protocol no. 130208393). Mice were housed in a pathogen-free environment at the facility of the University of Alabama at Birmingham.

Materials

Unless stated otherwise, the molecular biology-grade chemicals were purchased from Millipore-Sigma (St. Louis, MO, USA) or Fisher (Atlanta, GA, USA) companies. The Rabbit polyclonal anti-human aquaporin-0 (AQP0) antibody was purchased from Alpha Diagnostics (San Antonio, TX, USA). Additional commercial sources of various chemicals and antibodies used in the study are described throughout the text.

Generation of Transgenic Mice

The mouse model that expresses a human αA-crystallin gene in which Asn-101 was replaced with Asp is referred to as αA_{N101D}-transgenic mouse model. This model has been considered to be “deamidated” in this study, and the mice expressing αAN101D-transgene is referred here as CRYαA_{N101D} mice. Both mouse models (human lens αA_{N101D} transgenic- and human wild-type αA-transgenic mouse models were generated in Dr. Om Srivastava’s laboratory [28]. Independent transgenic (Tg) mouse lines were established from transgenic founders using C57BL/6 mice (Harlan Laboratories, Indianapolis, IN). αAN101D protein expression constituted about 14% and 14.2% of the total αA in the lens WS-and WI-proteins of the αA_{N101D} transgenic mice, respectively [28]. The mouse lenses were extracted after the mice were euthanized using the CO_2 procedure as per approved method by the Institutional Animal Care and Use Committee (IACUC) of the University of Alabama at Birmingham (Protocol no.130208393). Adult (2–3 months) wild type mice (C57BL6) were obtained from the university breeding colony. Animals were kept under a 12/12 h light–dark cycle and had *ad libitum* access to food and water. We have used three mice from each group of CRYαA_{WT} mice control and αA_{N101D} mice in all the experiments described below.

Isolation of Water Soluble (WS)- and Water Insoluble (WI)-Proteins from Mouse Lenses The WS- and WI-protein fractions from lenses of desired ages of CRYαA_{WT}- and CRYαA_{N101D} mice were prepared as previously described by us [28]. All procedures were performed at 5°C unless specified otherwise. The lenses were removed under a dissecting microscope and placed in 5°C-cold buffer A (5 mM Tris-HCl, 1 mM EDTA, 1 mM DTT, pH 7.8, and protease inhibitor cocktail [Roche Life Science, Indianapolis, IN]), and centrifuged at 14,000 x g for 15 min at 5°C to separate the WS- and WI- protein fractions. The supernatant (WS-protein fraction) was collected, and next the pellet (WI-protein fraction) was resuspended in buffer A, centrifuged as above. The recovery of WS- and WI-protein fractions was repeated twice after centrifugation, and the WS supernatants after each centrifugation steps were pooled. The final WI-protein pellet was solubilized in 5 mM Tris-HCl, pH 7.5, containing 8 M urea, 5 mM EDTA, and 5 mM EGTA. The 8 M urea concentration was diluted to 4 M urea with buffer A prior to centrifugation as above. The protein

concentrations in these fractions were determined by using a kit (Pierce Biotechnology-Thermo Fisher) using bovine serum albumin as a standard.

Membrane Isolation from Mouse Lenses

The membranes from lenses of 1- and 6-month-old CRYαA$_{WT}$ and CRYαA$_{N101D}$ mice were prepared as described previously [30, 31]. Lenses of identical ages from both types of mice were homogenized in buffer B (0.05 M Tris-HCl, pH 8.0 containing 5 mM EDTA, 1 mM DTT, 150 mM NaCl, and protease inhibitor cocktail [Roche, Indianapolis, IN]), and the preparations were centrifuged at 100,000 x g for 30 min using Beckman TL 100 centrifuge with a TLA 100.3 rotor. The supernatant was collected, and the pellets were washed twice with the above buffer B and centrifuged as above. This was followed by three additional washes with buffer B containing 8 M urea and centrifugation as above after each wash. Next, the pellet was washed twice with water and centrifuged as above. The pellet was then washed with 0.1 M cold (5^0C) NaOH [30, 31]. A final wash of pellet was with water and centrifugation as above to recover the purified lens membrane preparations as pellets.

Purification of Recombinant WTaA- and aA-$_{N101D}$-crystallins, their Conjugation with Alexa Fluor 350 and Membrane Binding

The WTaA- and aA-N101D mutant proteins were expressed in *E.coli* and purified by a Ni-affinity column chromatographic method as previously described by us [28]. Each protein was labeled with Alexa-350 using a protein labeling kit as suggested by the manufacturer (Molecular Probes, Carlsbad, CA).The binding of Alexa 350-conjugated WT aA- and aA-N101D mutant proteins to mouse lens membrane (isolated from C57BL non-transgenic mice) was determined as previously described [32, 33]. During the binding assay, the purified lens membrane (containing 2.5 mg protein; isolated from 1 to 3-month old non-transgenic C57 mice) was incubated with increasing but identical concentrations of either Alexa-labelled WT aA- or aA-$_{N101D}$ proteins at 37^{o}C for 6 h. Next, the incubated preparations were centrifuged at 14,000 X g and the supernatant and pellet (membrane fraction) recovered. After washing the membrane fraction with water and centrifugation as above, the relative levels of fluorescence of membranes incubated with WT aA- and aA-$_{N101D}$ mutant proteins were determined using Perkin Elmer Multiplate Reader (Model Victor1420-04).

Determination of Intracellular Ca^{2+} in Epithelial Cells in Culture from Lenses of CRYαA$_{WT}$ - and CRYαA$_{N101D}$ Mice

To culture epithelial cells, six 5-months old lenses from CRYαA$_{WT}$ - and CRYαA$_{N101D}$ mice were excised and incubated with 0.25% trypsin at 37^o C for 2.5 h in an incubator with 5% CO_2-humidified air. Next, the lens cells in trypsin solution were centrifuged at 1200 rpm for 3 min, and trypsin (in the supernatant) was discarded. The lens epithelial cells (recovered as pellet) were suspended in medium 199 (Thermo Fisher Scientific, Grand Island, NY) containing 10% fetal calf serum (Hyclone, Logan, Utah) and 1% antibiotic-antimycotic solution (Thermo Fisher Scientific, Grand Island, NY) in 12-well plates (Corning, Franklin

Lakes, NJ). After 24 h, the unattached cells were discarded by washing with the above medium. The old medium was replaced with fresh medium after every 48 h, and the cells were allowed to grow for 7 to 10 days until confluent. Next, the confluent cells were trypsinized and seeded in 12-well plates for intercellular Ca^{2+} determination and were allowed to grow for 24 h. The cells were washed with medium 199 without phenol red, incubated in calcium orange dye (Thermo Fisher Scientific, Grand Island, NY) at a final concentration of 4 μM for 30 min at room temperature as instructed in the manufacturer's protocol. After 30 min, the cells were washed with the above medium, and Ca^{2+} indicator was examined under a microscope (Leica DMI 4000B) using a Texas Red filter.

Western Blot and Immunohistochemical Analyses

The WS- and WI-proteins and membrane fractions isolated from lenses were analyzed for their immunoreactivity with anti-aquaporin-0 antibody (to visualize the membrane intrinsic protein), and Mouse anti-His monoclonal antibody ([Novagen, Madison, WI], to visualize WTαA and $αA_{N101D}$) during Western blot analysis. The SDS-PAGE analysis was carried out as described by Laemmli [34].

The confocal immunohistochemical analysis of lens axial sections of WTαA and $αA_{N101D}$ was carried out as previously described by us [28]. The analysis was performed at the High-Resolution Imaging core facility of the University of Alabama at Birmingham.

Localization by Immunohistochemical-Transmission Electron Microscopic Method

The analysis was performed at the High-Resolution Imaging core facility of the University of Alabama at Birmingham. His-tagged $αA_{WT}$- and $αA_{N101D}$-crystallins were localized in lens cells by an Aurion immunogold method and the reagents used were Aurion Conventional Immunogold reagents (Electron Microscopy Science [PA]). Lenses of desired ages were fixed in phosphate-buffered saline, pH 7.4 containing 4% paraformaldehyde and 0.05% glutaraldehyde (Electron Microscopy Sciences, Hatfield, PA) for 2 h at room temperature, and then overnight at 4°C. The fixed lenses were washed with water (Millipore, Billerica, MA). Samples were dehydrated by ascending ethanol gradient series followed by infiltration overnight at 4°C with absolute ethanol: London Resin (LR) white (1:1). Next, the samples were incubated overnight with pure LR white resin on a rotating platform. The lenses were removed and transferred to gelatin capsules containing fresh LR white and allowed to polymerize for 24 h at 45-50°C. Ultra-thin (silver gold to light gold) LR white lens sections were collected on nickel mesh grids. The color of sections was silver-gold to light gold, and based on their color, the thickness was estimated to between 70-80 nm. For immunogold-labeling, the protocol as described in Electron Microscopy Sciences (Hatfield, PA) was precisely followed. To inactivate aldehyde groups present after aldehyde fixation, the samples on grids were incubated on 0.05 M glycine in PBS buffer for 10-20 minutes. Next, the grids were transferred onto drops of the matching Aurion blocking solution for 15 min, and then were washed for 15 min in incubation solution (PBS containing 0.1% bovine serum albumin and 15 mM NaN3, pH 7.3). This was followed by a 2X wash in incubation buffer, each time for 5 min. The grids were incubated with two primary antibodies (Mouse anti-His monoclonal antibody and Rabbit anti-aquaporin-0 polyclonal

antibody for 1 h. In controls, the primary antibodies were omitted. The grids were then washed 6X (5 minutes each time) with the incubation solution and transferred to following secondary antibody conjugates {(goat anti-Rabbit EM grade conjugate 25 nm diameter) and (goat anti- mouse EM grade conjugate 10nm diameter)} and were incubated for 30 minutes to 2 h. The grids were washed on drops of incubation solution for 6X (5 min each time). The grids were washed twice with PBS for 5 min, post-fixed in 2% glutaraldehyde in PBS for 5 min, and finally washed with distilled water and contrasted according to standard procedures. Lens sections were imaged using an FEI 120kv Spirit TEM (FEI-Thermo Fisher), and images were collected using an AMT (AMT-Woburn, MA) digital camera.

RNA Extraction and Reverse Transcription-Quantitative Polymerase Chain Reaction (RT-PCR [qPCR])

RNA was extracted with Trizol reagent (Invitrogen) from cultured lens epithelial cells from CRYαA$_{N101D}$ and CRYαA$_{WT}$ mice, and all the samples were analyzed in triplicates. Real-time PCR quantifications were performed using the BIO-RAD iCycler iQ system (Bio-Rad, Hercules, CA), using a 96-well reaction plate for a total volume of 25 µL. RNA was extracted as described above. Primers were designed using Primer3 for the following genes:

Atp1a2 Forward-5'CGGGAGCCATAAGGGTTTGT 3', and **Atp1a2** Reverse- 5'GCACTGACTTGGCTGTTGTG 3'

The ACTB gene was used for normalization. The reaction mixture included 12.5 µL of Real- Time SYBR Green PCR master mix, 2.5 µL of reverse transcription product, 1 µL of forward and reverse primer and 8 µL of DNase/RNase free water. The reaction mixtures were initially heated to 95ºC for 10 min to activate the polymerase, followed by 40 cycles, which consisted of a denaturation step at 95ºC for 15 sec, annealing at 55ºC for 60 sec and an elongation step at 72ºC. The qRT-PCR data were analyzed by the comparative ΔCt method.

Results

Age-Related Protein Insolubilization in Lenses of CRYαA$_{N101D}$ and CRYαA$_{WT}$ Mice

To determine at what age there is change in the protein profiles in lenses of CRYαA$_{N101D}$ and CRYαA$_{WT}$ mice occurred, a comparative analysis of WS-proteins and WI-proteins from the lenses of the two types of mice of different ages was carried out *(*Fig. 1). The WS- and WI-proteins from lenses of different ages (1-, 3-, 4-, 5- and 7-months) were analyzed by SDS-PAGE. The WS-protein profiles from the lenses of the CRYαA$_{N101D}$ and CRYαA$_{WT}$ mice were almost identical until 3-months of age, except lens preparations from ages of 4-, 5- and 7-months of CRYαA$_{N101D}$ mice exhibited relatively greater levels of aggregated protein of M_r >30 kDa and higher relative to same-aged lenses from CRYαA$_{WT}$ mice (Lanes 4 and 5 in Figure 1B). Additionally, on quantification, the relatively increasing levels of WS-proteins showed age-related water insolubilization beginning at 4-months of age in the lenses of αA$_{N101D}$ mice (Table 1). Between 4- to 7-months of age, relatively about 5 to 10% higher proteins became insoluble in lenses of CRYαA$_{N101D.}$To determine changes in individual crystallins due to their insolubilization, the WS-protein

fraction from 7-month-old lenses was fractionated by a size-exclusion HPLC using a G-4000PWXL column (Tosoh Biosciences, fractionation range of protein with M_r's between $1X10^4$ to $1X10^7$ Da). The comparative protein elution profiles at 280 nm of 7-month old lenses of αA_{N101D}-mice showed an increased protein in the void volume peak (representing WS-HMW proteins), and reduced β- and γ-crystallin peaks relative to lenses of CRYαA_{WT}-mice (the differences shown in green in Figure 2A). The void volume peak in WS-protein fraction was also higher in the 7-month old lenses relative to 1-month old lenses of αA_{N101D}-mice (Results not shown), suggesting a relatively increased HMW protein aggregate formation with aging. On western blot analysis of the individual column fractions nos. 6 to 9 (constituting the void volume-HMW-protein peak) with an anti-His antibody, the levels of His-immunoreactive protein were higher in 7-month old CRYαA_{N101D} lenses compared to the identical aged CRYαA_{WT} lenses (Figure 2B). Additionally, because the immunoreactive peak in the WT lenses was in the fractions no. 8 and 9 whereas it was in the fractions no. 7 and 8 in the αA_{N101D} lenses that suggested that the HMW proteins of αA_{N101D} lenses showed a higher molecular weights relative to the HMW proteins from WT lenses. On quantification of Western blot images with Image J (Figure 2C), the intensity of the immunoreactive HMW proteins of αA_{N101D} was about 20% greater relative to WT lenses. Together, the results suggested a greater aggregation with higher M_r of the HMW-proteins in CRYαA_{N101D} lenses compared to the identical aged CRYαA_{WT} lenses.

Identification Proteins Present in Water Insoluble-Urea Soluble (WI-US) - and Water Insoluble Urea Insoluble (WI-UI) Protein Fractions of Lenses of CRYαA_{WT} and CRYαA_{N101D} Mice

To Identify the insolubilized proteins in WTαA vs. αA_{N101D} lenses, the WI-proteins from 5-month-old mice were further fractionated into WI-US- and WI-UI-protein fractions, and examined by SDS-PAGE (Figure 3) followed by their protein compositional analysis by mass spectrometry. SDS-PAGE analysis showed that both WI-US- and WI-UI-protein fractions from CRYαA_{N101D} lenses contained greater levels of protein species including aggregated proteins (M_r > 30 kDa) [Identified as a, and c in Figure 3] relative to the same fractions from lenses of CRYαA_{WT} mice (Identified as b and d in Figure 3). The mass spectrometric analysis was carried out at the following two levels: (i) In the first level analysis, determination of the total protein compositions in the WI-US- and WI-UI protein fractions of the two types of lenses (Supplemental Tables A [Comparative protein compositions of WI-US-fractions of CRYαA_{N101D} and WTαA lenses], and Supplemental Table B [Comparative protein compositions of WI-UI-fractions of αA_{N101D} and WTαA lenses]). (ii) In the second level analysis, the protein compositions of protein aggregates (M_r >30 kDa) in WI-US-fraction of αAN101D lenses (Identified as 'a' in Figure 3), and WI-US-protein fraction of WTαA lenses (Identified as 'b' in Figure 3) [Supplemental Table C]. Similarly, the compositions of protein aggregates (M_r >30 kDa) in WI-UI-fraction of αA_{N101D} lenses (Identified as 'c' in Figure 3,), and WI-US-fraction of WTαA lenses (Identified as 'd' in Figure 3) were determined [Supplemental Table D]. The rationale of the two levels of analysis was to determine the relative proteins compositions due to the greater insolublization of proteins in CRYαA_{N101D} lenses relative to CRYAAWT lenses (Figure 1, Table1). Our expectation was that the level 1 comparative examination would identify the total proteins that

underwent insolubilization, and existed in the US- and UI-protein fractions, whereas the level 2 analysis would selectively identify those proteins that formed aggregates (M_r >30 kDa) in the US- and UI-fractions. The rationale was that the information would implicate potential roles of specific crystallins in the aggregation and therefore, in the cataractogenic mechanism.

(i) Comparative Protein Compositions in WI-US Fractions of Lenses from CRYαA$_{N101D}$ and CRYαA$_{WT}$ Mice

The proteins detected in the WI-US-protein fractions of CRYαA$_{N101D}$ lenses but were absent in the *WT* lenses are described in Supplemental Table A. Together, the results show that the WI-US fraction of CRYαA$_{N101D}$ lenses was enriched in several histones, which could be due to the lack of denucleation relative to *WT* lenses. Absence of Retinal dehydrogenase in transgenic lens fraction.

(ii) Comparative Protein Compositions of WI-UI-Fractions of Lenses from CRYαA$_{N101D}$ and CRYαA$_{WT}$ Mice

The proteins present in the WI-UI-protein fractions of CRYαA$_{N101D}$ lenses but were absent in WT lenses are described in Supplemental Table B. In summary, the results again show that the majority of histones that existed in CRYαA$_{N101D}$ lenses were absent in the WT lenses, which could be due to the lack of denucleation in the lenses of former mice. Also, specifically αB- and βB2-crystallin became insoluble as their levels were higher even in the WI-UI-fraction of lenses of CRYαA$_{N101D}$ relative to WT lenses.

(iii) Compositions of Aggregated Proteins (M_r >30 kDa) in WI-US- and WI-UI-Fractions of Lenses from CRYαA$_{N101D}$ and CRYαA$_{WT}$ Mice

As noted above, the purpose of the second level of mass spectrometric analysis was to elucidate the comparative compositions of aggregated proteins (M_r >30 kDa) in WI-US- and WI-UI-protein fractions of CRYαA$_{N101D}$ and CRYαA$_{WT}$ lenses [Supplemental Tables C and D]. On comparison, the major proteins present as aggregates (M_r > 30 kDa) in WI-US fraction of CRYαA$_{N101D}$ but absent in CRYαA$_{WT}$ were (Supplemental Table C): βB3- and γC-crystallins, collagen alpha-1(IV) chain and -alpha-2(IV) chain and nestin. In contrast, the exclusively present major proteins in WI-US fraction of CRYαA$_{WT}$ were: γC-, γD-, γE-γF-crystallins. The above list describes the selective proteins that were water insoluble-urea soluble and became the part of the complexes with M_r > 30 kDa in CRYαA$_{N101D}$ lenses. The greater abundance of αA-, and βB1-crystallins in the aggregated form suggested their potential involvement in the aggregation process along with βB3- and γC-crystallins.

On comparison of major proteins that existed in WI-UI protein fraction as > 30 kDa aggregates in CRYαA$_{N101D}$ not in the CRYαA$_{WT}$ included [Supplemental Table D]: γB-, γD- and γE-crystallins, and nestin. In the WI-UI fraction, the greater abundance of proteins in CRYαA$_{N101D}$ compared to CRYαA$_{WT}$ were: αA-crystallin and lens fiber intrinsic proteins. Together, the results showed that the proteins that remained urea insoluble and were possibly associated with the membrane of CRYαA$_{N101D}$ lenses included: γB-, γD- and γE-crystallins, and nestin (Nestin is an intermediate filament protein).

Increased Association of αAN101D with Lens Membrane in the Outer Cortical Fiber Cells relative WTαA in CRYYAAWT lenses

Our previous report [28] showed an increased levels and abnormal deposition of αA_{N101D} within the outer cortical region in CRYαA$_{N101D}$ lenses compared CRYαA$_{WT}$ lenses. This suggested a relatively greater membrane binding of $\alpha A_{N101D,}$ which was further investigated in experiments as described below.

(i) Immunohistochemical Analyses of Lenses from CRYαA$_{N101D}$ and CRYαA$_{WT}$ Mice

The purpose of the experiments was to determine relative levels of αAN101D and WTαA in the outer cortical regions of CRYαA$_{N101D}$- vs. CRYαA$_{WT}$ lenses. This was examined by immunohistochemical analysis of 5-months old lenses of the two types of mice using anti-His monoclonal (for detection of WTaA and aA_{N101D} [green fluorescence]) - and polyclonal anti-aquaporin 0 (for membrane detection [red fluorescence])-antibodies (Figure 4). The axial sections (at 10X magnification) showed an irregular and greater deposition of His-tagged aA (Green) in the lens outer cortex of CRYαA$_{N101D}$ mice (Shown by an arrow in Figure 4A) relative to CRYαA$_{WT}$ mice (Shown by an arrow in Figure 4B). Similarly, the equatorial sections (at 40X magnification) also exhibited a greater immunoreactive green fluorescence in the outer cortex of the CRYαA$_{N101D}$ lens relative to the CRYαA$_{WT}$ lens (shown by arrows in Figure 4C and D). Together, the results suggested the abnormally greater levels of association of αA_{N101D} in the outer cortical regions, and potentially with the fiber cell membranes in the CRYαA$_{N101D}$ lenses relative to those of CRYαA$_{WT}$ lenses.

(ii) Relative Membrane-Association of WTαA- and αA_{N101D} in Lenses of CRYαA$_{N101D}$ and CRYαA$_{WT}$ Mice

The rationale for the next experiment was that if the greater membrane-association of $\alpha A\text{-}_{N101D}$ occurs *in vivo* in CRYαA$_{N101D}$ lenses compared to CRYαA$_{WT}$ lenses, the difference in their levels could also be determined in the purified membrane fractions by western blot analysis. The expectation was that following the step-wise membrane purification by using 8M urea (to dissociate non-covalently-bound membrane proteins), and by the final wash with 0.1N NaOH (to remove non-membranous extrinsic proteins) [30, 31], the purified membrane would show relative levels of membrane-association of αA_{N101D} vs. WTαA in the two types of mice. To normalize the levels of the relative association during the membrane preparations, two lenses of 1-month-old and two lenses from 6-month old from CRYαA$_{N101D}$ and CRYαA$_{WT}$ mice were identically processed, using identical volumes of buffers at each steps during membrane purification (See Methods). Next, Western blot analysis using anti-His- and anti-aquaporin 0-antibodies were used to determine the relative levels of membrane-association of WTαA and αAN101D at different purification steps (Results not shown). To simplify the western blot results of fractions recovered during the sequential steps of membrane purification, only the results of immunoblots with anti-His antibody but not with anti-aquaporin-0 are shown in Figure 5. However, the western blot profiles with anti-aquaporin-0 were almost identical to anti-His antibody results. In Fig. 5, A, B, E and F show SDS-PAGE analysis followed by Coomassie blue-stained gels exhibiting relative levels of protein bands in

preparations at different membrane purification steps in lenses at two different age groups (1 and 6 months). In Fig. 5, C and D (1-month old lenses) and G and H (6-months old lenses) corresponded to samples of A, B, E and F (Coomassie blue-stained gels), and show the Western blot results with anti-His antibody (green fluorescence) in the two different age groups (1 and 6 months). The levels of green fluorescence with His-tagged αA in lenses of 1-month old lenses (Figure 5, left panel: WTαA [C] and αA_{N101D} [D]) and 6-month old lenses (Figure 5, right panel: WTαA [G] and αA_{N101D} [G]) are shown. Additionally, in both left and right upper panels, the lanes 1, 2 and 3 show the WS-protein fractions recovered after first, second and third consecutive washes in buffer A to solubilize WS-proteins, respectively. Lanes 4 and 5 represent the urea soluble-protein fractions recovered during two consecutive washes of WI-protein pellet (containing membranes) with buffer B containing 8M urea, respectively. Lane 6 represents the 0.1N NaOH-solubilized proteins from membranes and the lane 7 from both 1- and 6-month old lenses (left and right panels) show the purified lens membrane preparations. Similarly, lanes 7 and 8 from 6-month old lenses (right panel) represent purified membrane preparation. Lane 9 of 6-month old lenses represents the crude lens WS-homogenate. The results show that the green fluorescence representing WTαA in $CRY\alpha A_{WT}$ mice was entirely disappeared on urea solubilization in 1- and 6-month old lenses (lanes 1 to 5 in both left and right panels), whereas it was still present in these lenses until 0.1N NaOH wash (lane 6 in left and right panels). In contrast, the green fluorescence still existed in lane 6 of membranes from 1- and 6-month-old $CRY\alpha A_{N101D}$ lenses. Together, the results suggest that αA_{N101D} was tightly bound and at the higher levels to lens membrane of $CRY\alpha A_{N101D}$ lenses relative to $CRY\alpha A_{WT}$ lenses.

On Image J-quantification of the Western blots (Figure 5 I and J), the lanes 4 and 5 (urea soluble fractions) of 1-month old lenses showed higher levels (2.5X) of immunoreactivity with anti-His antibody in the $CRY\alpha A_{N101D}$ lenses (shown in red) compared to those from $CRY\alpha A_{WT}$ lenses (blue). Similarly in Figure 5J, among the lanes 4 and 5 containing same fractions from 6-month old lenses (as described in 1-month old lenses), the lane 5 showed a greater immunoreactive level of $CRY\alpha A_{N101D}$ lenses (red) compared to $CRY\alpha A_{WT}$ lenses (blue). Additionally, the lane 6 (representing membrane remaining after two urea washes, right panel) of 6-month $CRY\alpha A_{N101D}$ lenses exhibited about 2X greater immunoreactivity than $CRY\alpha A_{WT}$ lenses (Quantification results not shown). Together, the results show that relative to $CRY\alpha A_{WT}$, higher levels of $CRY\alpha A_{N101D}$ were tightly associated with the lens membranes of 1- and 6-month old $CRY\alpha A_{N101D}$ mice.

(iii) Relative Membrane-Binding of Alexa 350-Labeled Recombinant WTaA- and aA_{-N101D} Crystallins To examine whether αA_{N101D} show a greater binding affinity to the lens membrane relative to WTaA-crystallin, the binding of the two recombinant proteins to purified lens membrane was determined. The recombinant WTaA- and aAN101D proteins were labeled with Alexa 350 using a protein labeling kit by the procedure described by the manufacturer (Molecular Probes, Thermo fisher Scientific). The two labeled-proteins were purified by a size-exclusion HPLC column and were analyzed by SDS-PAGE. Figure 6A shows the Coomassie blue-stained WT aA (lane 1), aA_{N101D} protein (lane 2), and the purified lens

membrane from non-transgenic C57 mice (lane 3). The Figure 6B shows the images of the two Alexa 350-labeled proteins under a UV trans-illuminator [Lane 1: Images of Alexa 350-labeled WTaA, and lane 2: Alexa 350-labeled aAN101D). During the binding assay, the purified lens membrane (containing 2.5 mg protein; isolated from 1 to 3-month old non-transgenic C57BL mice) was incubated with increasing but identical concentrations of either Alexa-labelled WT aA- or aA_{N101D} proteins at 37^{o}C for 6 h (See details in Methods). A relatively higher levels (> 1.5X) of binding of aAN101D protein relative to WTaA protein with membrane preparation was observed (Figure 6C). The values reported are the average of triplicate assays.

(iv) Immunogold-Labeling for Relative Localization of αA-WT and αAN101D in Lens Membranes of CRYαA$_{N101D}$ and CRYαA$_{WT}$ Mice

To ascertain the relative levels association αAN101D vs. WTαA to the lens membrane *in vivo*, the immunogold-labeling experiment was carried out (See details in Methods). (A) and (B) in Figure 7 show lens membranes from CRYαA$_{N101D}$ and CRYαA$_{WT}$ mice at 500 nm magnification, and (C) and (D) from these lenses at 100 nm magnification, respectively. The bigger gold particles (25 nm, red arrows) the smaller gold particles (10 nm, yellow arrows) represented the aquaporin-0 and the His-tagged αAN101D and WTαA, respectively. As shown in the representative images in (A) to (D), the 25 nm gold particles (representing aquaporin-0, identified by red arrows) were bound to membranes. On counting the membrane-associated 10 nm particles (representing His-tagged αAN101D and WTαA), almost the same numbers of the particle were found to be associated with membranes of both CRYαA$_{N101D}$ and CRYαA$_{WT}$ lenses, suggesting that the His-tagged αAN101D and WTαA were bound to the membranes of the two types of lenses. Our previous study [28] showed that αAN101D protein constituted about 14% and 14.2% of the total αA- crystallin in the WS- and WI-proteins, respectively in the lenses of CRYαA$_{N101D}$ mice. Therefore, an argument can be made that although an almost equal number of 10 nm and 25 nm particles were associated with membranes of the two type of lenses, a higher number of gold particle representing αAN101D relative to WTαA were associated with the membrane.

Another interesting observation was that the membranes of CRYαA$_{N101D}$ lenses were about 2X more swollen relative to those of CRYαA$_{WT}$ lenses [Figure 7, compare (A) to (B) and (C) to (D)]. The width of the membrane was quantified using Image J as shown in Figure 7E. The swelling could represent water intake within the lens cells due to the potential ionic imbalance in the CRYαA$_{N101D}$ lenses compared to CRYαA$_{WT}$ lenses. Such a possibility of ionic imbalance was further determined as described below.

Na, K-ATPase and Ca^{2+} Levels in Cultured Epithelial Cells from Lenses of CRYαA$_{N101D}$ and CRYαA$_{WT}$ Mice

Sodium-potassium-adenosine triphosphatase (Na, K-ATPase) has been recognized for its role in regulating electrolyte concentrations in the lens, and the electrolyte balance is vital to lens transparency [35, 36]. In addition, calcium has been reported to control both sodium and potassium permeability through lens membranes [37]. In our previous study [29], we showed that the expression of Na,K-ATPase

at the protein level was drastically reduced in CRYαA$_{N101D}$ lenses relative to CRYαA$_{WT}$ lenses. Next, the levels of Na, K-ATPase mRNA, and Ca^{2+} levels were determined in cultured epithelial cells from lenses of CRYαA$_{N101D}$ and CRYαA$_{WT}$ mice. Both (A) and (B) in Figure 8 show intracellular Ca^{2+} levels in the presence of calcium orange in cultured epithelial cells from CRYαA$_{N101D}$ and CRYαA$_{WT}$, respectively. Only a few CRYαA$_{N101D}$ epithelial cells showed the Ca^{2+} uptake, which was possibly due to our previous finding that the lens cells contained only about 14% of αAN101D mutant protein [28]. In this experiment, 100 cells from the cultures of two types of lenses were counted. On quantification by Image J, the number of cells exhibiting calcium orange uptake were 1.5X greater in cells of CRYαA$_{N101D}$ lenses relative to cells from CRYαA$_{WT}$ lenses (Figure 8B). On the determination of levels of mRNA of Na, K-ATPase in these cells, its level was 75% lower in the CRYαA$_{N101D}$ lens cells than CRYαA$_{WT}$ lens cells (Figure 8C).

Discussion

Several past studies have shown *in vitro* effects of deamidation of crystallins on their structural properties including those in αA-, and αB-crystallins [21-25]. It has been reported that deamidation of Asn and Gln was the major modification identified in several human cataractous and aged lenses and these totaled 66% of the modification in the water-soluble and water-insoluble protein fractions that was analyzed by 2D LC/MS [38]. The mass spectrometric analysis found that there is negligible (less than 1%) deamidation at αA$_{N101}$ site in both aged and cataractous human lenses [39]. These studies suggested that because of low levels of deamidation of αA- at N101 to D in normal and cataractous lenses, the αAN101D might not play a significant role in cataract development. However, additional studies suggest otherwise. For example, our *in vitro* studies showed significant altered structural and functional properties of αA-crystallin on deamidation of N101 residue but not of N123 residue [24]. We also showed that the WS-protein fraction from 50-70 year-old human donors contained αA- fragments with deamidation of N101 to D [40]. This finding is significant because recent studies have also shown an increasing role of crystallin fragments in cataract development [41, 42]. In the present study, the cortical cataract development in mice on the introduction of αA-N101D transgene further show significance of deamidation of this site and altered changes in the lens. However, the exact *in vivo* molecular mechanism of αAN101D-induced crystallin's aggregation is yet to be fully understood.

Previously we showed that the three recombinant deamidated αA-mutants (N101D, N123D, and N101D/N123D) exhibited reduced levels of chaperone activity, alterations in secondary and tertiary structures, and larger aggregates relative to WT-αA-crystallin [24, 25]. Among the above three mutants, the maximally affected and altered properties were observed in the recombinant αAN101D mutant [25]. Additionally, our recent results show that *in vitro,* the deamidated αA-, and αB-crystallins facilitated greater interaction with βA3-crystallin, leading to the formation of larger aggregates, which might contribute to the lens cataractogenic mechanism [43]. As a further extension of our previous studies (28, 29]), in some studies the 7-month old lenses were chosen because of the development of cortical cataract at about 7-month of age in the αA-$_{N101D}$ mice relative to αA$_{wt}$ mice. In other experiments, lenses from 5-month old of

both types of mice were used to determine the progression of phenotypic changes in lenses to determine their significance in cataractogenic mechanism.

The present study show that the introduction of αAN101D trans-gene in a mouse model resulted in the following major *in vivo* effects in lenses of CRYαA$_{N101D}$- relative to CRYαA$_{WT}$ mice: (A) An age-related difference in protein profiles with an increasing association αA$_{N101D}$ with WI-protein fraction suggesting its insolubilization after 4-months of age. (B) The WS-HMW protein fraction showed a higher level of proteins with a greater M_r . (C) Mass spectrometric analysis showed preferential insolubilization of αA-, αB-, γD- and γE-crystallins, and nestin, which remained insoluble even in 8M urea. (D) The tight association of αAN101D with membranes relative to WTαA, which could not be fully dissociated with 8M urea treatment. (E) In vitro, αA$_{N101}$ a showed greater affinity and binding to lens membranes relative WTαA. (F) The greater number of immunogold-labeled αA$_{N101}$ relative WTαA binding to membrane along with relatively greater swelling of lens membranes, suggesting the potential water uptake due to intracellular ionic imbalance, and (G) The ionic imbalance was suggested by the greater Ca^{2+} uptake and 75% reduction in mRNA levels of Na, K-ATPase in the epithelial cells cultured from CRYαA$_{N101D}$ lenses relative to those from CRYαA$_{WT}$ lenses. Our mass spectrometry analysis showed that retinal dehydrogenase was absent in the N101D mice. It has been shown earlier that *Aldh1a1*(−/−) knock-out mice developed lens opacification later in life (44). Retinal dehydrogenase 1 may protect the lens against cataract formation by detoxifying aldehyde products on lipid peroxidation in both cornea and lens. It has been shown that antimalarial drug chloroquine which binds and inhibit retinal dehydrogenase 1 (45) induce cataract in rats (46). Together, these findings suggest altered membrane integrity (possibly due to greater levels of αA$_{N1010D}$ binding to membrane than WTαA) resulting in intracellular ionic imbalance in CRYαA$_{N101D}$ lenses, which could play a major role in the cortical cataract development.

Among the lens crystallins, only α-crystallin show an association with the membrane in both normal and cataractous lenses [6, 47-51]. Lens membranes contain both a high-affinity saturable and low-affinity non-saturable α-crystallin-binding sites [47, 51-53]. Alpha-crystallin binding to native membranes was enhanced on stripping of extrinsic proteins from the lens membrane surface to expose lipid moieties [32, 33], which contradicted a previous report that the crystallin mostly interacts with lens membrane MP26 protein [54]. Even after stripping extrinsic membrane proteins by alkali-urea treatment, the full-length αA-, and αB-crystallins remained associated with membranes of both bovine and human lenses [6]. Additionally, αB-crystallin showed three-fold higher binding to lens membrane relative to αA-crystallin, and their binding was affected by the residual membrane-associated proteins, suggesting that their binding behaviors were affected by an intrinsic lens peptides [6]. A large-scale association of proteins with cell membranes in the lens nucleus (mostly in the barrier region) occurs after middle age in human lenses [49], and such association was enhanced by mild thermal stress [50]. The *in vitro* studies further supported this because the binding capacity of α-crystallin from older lenses to lipids increased with age and decreased in diabetic donors who were treated with insulin [51]. This implied that under diabetic conditions, abnormal binding of α-crystallin to lens membrane occurred. Such information in the literature about membrane binding of native vs. post-translationally modified crystallins including the deamidated

αAN101D species is presently lacking. Therefore, the results of the present study showing relatively increased binding of αAN101D relative to WTαA are highly significant.

The RNA sequence and IPA data of our previous study [29] further support the findings of the present study. This study [29] showed that the genes belonging to gene expression, cellular assembly, and organization, and cell cycle and apoptosis networks were altered, and specifically, the tight junction-signaling and Rho A signaling were among the top three canonical pathways that were affected in the CRYαA$_{N101D}$ lenses relative to CRYαA$_{WT}$ lenses. The present study showed an increased association of αAN101D to membrane, and this could lead to potential ionic imbalance affecting tight junction assembly and RhoA GTPase expression. This in turn causes increased proliferation and decreased of differentiation and denucleation of epithelial cells, and an accumulation of nuclei and nuclear debris in the lens anterior inner cortex and fiber cell degeneration. Some of these phenotypic changes could be cause or effects, but together could be responsible for the age-related cortical cataract development in CRYαA$_{N101D}$ lenses.

To maintain ionic balance within lens cells, a permeability barrier close to the surface of the lens is responsible for the continuous sodium extrusion via Na, K-ATPase-mediated active transport [35-37]. Without an active sodium extrusion, lens sodium and calcium contents are shown to increase resulting in lens swelling that leads to loss of lens transparency [35]. Similarly, an excessive intracellular Ca^{2+} levels can be detrimental to lens cells, and its increased levels play an important role in development of cortical cataract [37]. Therefore, homeostasis of Na^{+}, $K^{+,}$ Ca^{2+} and other ions within the lens has been recognized as of fundamental importance in lens pathophysiology. These have been altered as shown in our present and our previous studies [29]. It is also possible that the increased Ca^{2+} levels could in turn lead to calpain activation and proteolysis of crystallins, which will be investigated in future.

Similar to our study, other studies have shown that an increased membrane binding of α- crystallin in the pathogenesis of different forms of cataracts. The high molecular weight complexes (HMWCs), comprised of α-crystallin and other crystallins, accumulate with aging and show a greater membrane binding capacity than native α-crystallin [51]. Other mutants of αA-crystallin, like the αA$_{N101D}$ mutant, also exhibit a greater membrane binding than corresponding wild-type species [55]. For example, in the αAR116C-associated congenital cataracts, an increased membrane binding capacity along with changes in complex polydispersity, and the reduction of subunit exchange were considered potential factors in the cataract pathogenesis [55]. Similarly, αA-crystallin R49C neo mutation influenced the architecture of lens fiber cell membranes and caused posterior and nuclear cataracts in mice [56].

Interactions between proteins and the cell membrane are an integral aspect of many biological processes, which are influenced by compositions of both membrane lipids and protein structure [57]. Reports have shown the age-related lipid compositional changes in the lens membrane, which might affect α-crystallin binding, i.e., in the nucleus of the human lenses, the levels of glycerophospholipids declined steadily by age 40 as opposed to the levels of ceramides and dihydroceramides increased approximately 100 fold during middle-age [58, 59]. Further, it has been shown that because of the elevation of sphingolipid levels

with species, age, and cataract, lipid hydrocarbon chain order, or stiffness increased. Therefore, the increased membrane stiffness caused an increase in light-scattering, reduced calcium pump activity, altered protein-lipid interactions, and perhaps slow fiber cell elongation [60]. Presently, whether similar changes occur in αA_{N101D} lenses are not known.

Alpha A- and αB-crystallins differently associate with the cellular membrane, i.e. αA-crystallin may interact exclusively with membrane phospholipids, and thereby unaffected by the presence of extrinsic proteins on the membrane, whereas these proteins may act as conduits for αB-crystallin to bind to the membrane [59]. Presently, the specific binding mechanism of αAN101D to the membrane and age-related changes in lipid composition in lenses CRYαA_{N101D} vs. CRYαA_{WT} are unknown, and these are presently the focus of our investigations.

Conclusions

The results presented in this study suggest that an increased association of αAN101D relative WTαA with the lens membrane causes a possible loss of membrane integrity, leading to an ionic imbalance, and in turn, to membrane swelling, cellular disorganization and finally cortical opacity. Our future study will determine the specific binding site in the αAN101D relative WTαA, and changes in the membrane compositions that might facilitate the increased binding of the deamidated crystallin with the membrane.

Abbreviations

CRYαA_{WT}: Wild-type alpha-A crystallins

CRYαA_{N101D}: Alpha-A-crystallin in which Asparagine (N) at 101 position was replaced with

Aspartic acid (D)

Atp1a2: ATPase Na+/K+ transporting subunit alpha 2

Na, K-ATPase: Sodium-Potassium-Adenosine triphosphatase

HMW: High Molecular Weight

His-tagged: Histidine tagged

WI-US: Water Insoluble-Urea Soluble

WI-UI: Water Insoluble-Urea Insoluble

Aldh1a1: Aldehyde Dehydrogenase 1 Family Member A1

SDS-PAGE: Sodium dodecyl sulfate- polyacrylamide gel electrophoresis

Declarations

Ethics approval and consent to participate

No human subjects were involved in the study. All animal experiments were performed per protocols approved by the Institutional Animal Care and Use Committee (IACUC) of the University of Alabama at Birmingham (Protocol no. 130208393). Mice were housed in a pathogen-free environment at the facility of the University of Alabama at Birmingham.

Consent for publication

Not applicable

Availability of data and materials

The datasets analyzed in the current study are available from the corresponding author for reasonable requests.

Competing interests

No competing interest

Funding

This study was funded by NIH grants, EY- 06400 (OS) and P30EY003039.

Authors' contributions

KS and RJ conducted experiments, analyzed and interpreted the data and wrote the manuscript. LW conducted the mass spectrometric analysis and analyzed and interpreted the results. OS with the help of RJ analyzed and interpreted the data, and have written and edited the manuscript.

Source of Animals

The CRYαA$_{N101D}$ mouse model was generated by inserting the human lens αA-N101D transgene and the CRYαA$_{WT}$ mouse was generated by inserting human wild-type αA-transgene. Both mouse models were generated in Dr. Om Srivastava's laboratory. The details of the methodology are described in reference no. 28 (Gupta R, Asomugha CO, Srivastava OP. The common modification in αA-crystallin in the lens, N_{101D} is associated with increased opacity in a mouse model. J Biol Chem. 2011; 286:11579-592)

Acknowledgements

Authors thank Ms. Rebecca Vance for the help with handling the CRYαA$_{N101D}$ and CRYαA$_{WT}$ mice. Thanks also goes to the High Resolution Imaging Facility, Targeted Metabolomics & Proteomics

Laboratory and the Ocular Phenotyping and Molecular Analysis Core Facility of Vision Science Research Center at the University of Alabama at Birmingham

ARRIVE Guidelines

Minimum Standard of Reporting Checklist

Experimental design and statistics

The method section contains the information as described in the guideline.

Resources

The description of all the resources used are included in the Method section.

Availability of data and materials

The datasets analyzed in the current study are available from the corresponding author for reasonable requests.

References

1. Mathias RT, TW White, X Gong. Lens gap junctions in growth, differentiation, and homeostasis. Physiol Rev. 2010;90:179-206.
2. Wride MA. Lens fibre cell differentiation, and organelle loss: many paths lead to clarity. Philosophical Transactions of the Royal Society of London B: Biol Sci. 2011; 366:1219-33.
3. Sharma KK, Santhoshkumar P. Lens aging: Effects of crystallins. Biochimica et Biophysica Acta-General Subjects. 2009;1790:1095-1108.
4. Stewart DN, Lango J, Nambiar KP, Falso MJS, FitzGerald PG, Rocke DM, Hammock BD, Buchholz BA. Carbon turnover in the water-soluble protein of the adult human lens. Mol. Vis. 2013;19:463-75.
5. Beebe DC, Holekamp NM, Siegfried C, Shui Y-Bo. Vitreoretinal influences on lens function and cataract. Philosophical Transactions of the Royal Society of London B: Biological Sciences 2011;366:1293-1300
6. Su S-P, McArthur JD, Friedrich MG, Truscott RJW, Aquilina JA. Understanding the α- crystallin cell membrane conjunction. Mol Vis, 2011;17:2798-2807.
7. Paterson CA, Delamere NA. ATPases and lens ion balance. Exp Eye Res, 2004;78:699- 703.
8. Vaghefi E, Beau P, Marc J, Donaldson P. Visualizing ocular lens fluid dynamics using MRI: manipulation of steady state water content and water fluxes. Am J Physiol-Reg, Integ Comp Physiol. 2011;301:R335-R342.
9. Borchman D, Yappert MC. Lipids and the ocular lens. J Lipid Res, 2010;51:2473-88.

10. Shiels A, Hejtmancik JF. *Chapter Twelve - Molecular Genetics of Cataract*, in *Progress in Molecular Biology and Translational Science*, J.F. Hejtmancik and M.N. John, Editors. 2015, Academic Press. p. 203-18.
11. Truscott RJW. Age-related nuclear cataract—oxidation is the key. Exp Eye Res, 2005;80:709-2512.
12. Harrington V, McCall S, Huynh S, Srivastava K, Srivastava OP. Crystallins in water soluble-high molecular weight protein fractions and water insoluble protein fractions in aging and cataractous human lenses. Mol Vis, 2004;10:476-89.
13. Harrington V, Srivastava OP, Kirk M. Proteomic analysis of water insoluble proteins from normal and cataractous human lenses. Mol Vis. 2007;13:1680-94.
14. Srivastava OP. Age-related increase in concentration and aggregation of degraded polypeptides in human lenses. Exp Eye Res. 1988;47:525-43.
15. Srivastava OP, McEntire JE, Srivastava K., Identification of a 9 kDa γ-crystallin fragment in human lenses. Exp Eye Res. 1992;54: 893-901.
16. Srivastava OP, Srivastava K, Silney C. Levels of crystallin fragments and identification of their origin in water soluble high molecular weight (HMW) proteins of human lenses. Curr Eye Res.1996:5:511-20.
17. Srivastava OP, Srivastava K. Degradation of γD- and γs-crystallins in human lenses. Biochem Biophys Res Commun. 1998;253:288-94.
18. Srivastava OP, Srivastava K, Harrington V. Age-related degradation of βA3/A1-crystallin in human lenses. Biochem Biophys Res Commun. 1999; 258:632-38.
19. Srivastava OP, Srivastava K. Existence of deamidated alpha B-crystallin fragments in normal and cataractous human lenses. Mol Vis. 2003;9:110-18.
20. Srivastava OP, Srivastava K. βB2-crystallin undergoes extensive truncation during aging in human lenses. Biochem Biophys Res Commun. 2003;31:44-49.
21. Srivastava OP, Srivastava K, Chaves JM, Gill AK. Post-translationally modified human lens crystallin fragments show aggregation in vitro, Biochem Biophys Rep. 2017;10:94-113.
22. Lampi KJ, Amyx KK, Ahmann P, Steel EA. Deamidation in human lens βB2-crystallin destabilizes the dimer. Biochemistry. 2006;45: 3146-53.
23. Wilmarth PA, Tanner S, Dasari S, Nagalla SR, Riviere MA, Bafna V, Pevzner PA, David LL. Age-related changes in human crystallins determined from comparative analysis of post-translational modifications in young and aged lens: Does deamidation contribute to crystallin insolubility? J Proteome Res. 2006;5:2554-66.
24. Gupta R, Srivastava OP. Deamidation affects structural and functional properties of human αA-crystallin and its oligomerization with αB-crystallin. J Biol Chem. 2004; 279: 44258-69.
25. Gupta R, Srivastava OP. Effect of deamidation of asparagine 146 on functional and structural properties of human lens αB-crystallin. Invest Ophthalmol Vis Sci. 2004;45: 206-14.

26. Rosenfeld L, Spector A. Changes in lipid distribution in the human lens with the development of cataract. Exp Eye Res. 1981; 6:641-650.
27. Harocopos GJ, Alvares KM, Kolker AE, Beebe DC, Human age-related cataract, and lens epithelial cell death. Invest Ophthalmol Vis Sci. 1998; 39:2696-2706.
28. Gupta R, Asomugha CO, Srivastava OP. The common modification in αA-crystallin in the lens, N101D is associated with increased opacity in a mouse model. J Biol Chem. 2011;286:11579-592.
29. Hegde SM, Srivastava K, Tiwary E, Srivastava OP. Molecular mechanism of formation of cortical opacity in CRYAAN101D transgenic mice cortical opacity in CRYAAN101D lenses. Invest Ophthalmol Vis Sci. 2014;55:6398-6408.
30. Wang Z, Han J, David LL, Schey KL. Proteomics and phosphoproteomics analysis of human lens fiber cell membranes. Invest Ophthalmol Vis Sci. 2013;54:1135-1143.
31. Tanaka M, Russell P, Smith S, Uga S, Kuwabara T, Kinoshita JH. Membrane alterations during cataract development in the Nakano mouse lens. Invest Ophthalmol Vis Sci.1980; 19:619-29.
32. Cobb BA, Petrash JM. Alpha-Crystallin chaperone-like activity and membrane binding in age-related cataracts. Biochemistry. 2002;41:483-490.
33. Cobb BA, Petrash JM. Characterization of α-crystallin-plasma membrane binding. J Biol Chem. 2000;275:6664-6672.
34. Laemmli UK. Cleavage of structural proteins during the assembly of the head of bacteriophage T4, Nature. 1970;227:680-685.
35. Delamere NA, Tamiya S. Lens ion transport: From basic concepts to regulation of Na, K-ATPase activity. Exp Eye Res. 2009;88:140-43.
36. Tseng SH, Tang MJ. Na,K-ATPase in lens epithelia from patients with senile cataracts. J Formosan Med Assoc. 1999;98:627-32.
37. Rhodes JD, Sanderson J. The mechanisms of calcium homeostasis and signalling in the lens. Exp Eye Res. 2009; 88:226-34.
38. Wilmarth PA, Tanner S, Dasari S, Nagalla SR, Riviere MA, Bafna V, Pevzner PA, David LL. Age-related changes in human crystallins determined from comparative analysis of post-translational modifications in young and aged lens: does deamidation contribute to crystallin insolubility? J Proteom Res. 2006;5:2554–2566.
39. Haines PG, Truscott RJW. Age-dependent deamidation of lifelong proteins in the human lens, Invest Ophthalmol Vis Sc. 2010;51:3107-3114.
40. Srivastava OP, Srivastava K, Chaves JM, Gill AK. Post-translationally modified human lens crystallin fragments show aggregation in vitro, Bioche Biophys Rep. 2017;102:94- 131.
41. Santhoshkumar P, Udupa P, Murugesan R, Sharma KK. Significance of interactions of low molecular weight crystallin fragments in lens aging and cataract formation. J Biol Chem. 2008;283:8477-485.
42. Srivastava K, Chaves JM, Srivastava OP, Kirk M. Multi-crystallin complexes exist in the water-soluble high molecular weight protein fractions of aging normal and cataractous human lenses. Exp Eye

Res. 2008;87:356-366

43. Lassen N, Bateman JB, Estey T et al. Multiple and additive functions of ALDH3A1 and ALDH1A1: cataract phenotype and ocular oxidative damage in Aldh3a1(-/-)/Aldh1a1(-/-) knock-out mice. J Biol Chem. 2007;282:25668–25676.
44. Graves PR, Kwiek JJ, Fadden P. Discovery of novel targets of quinoline drugs in the human purine binding proteome. Mol Pharmacol. 2002;62:1364–1372.
45. Drenckhahn D, Lullmann-Rauch R. Lens opacities associated with lipidosis-like ultrastructural alterations in rats treated with chloroquine, chlorphentermine, or iprindole. Exp Eye Res. 1977;24:621–632.
46. Tiwary E, Hegde S, Srivastava O. Interaction of βA3-crystallin with deamidated mutants of αA- and αB-crystallins. PLoS ONE, 2015, e0144621.
47. Chandrasekher G, Cenedella RJ. Properties of α-crystallin bound to lens membrane: Probing organization at the membrane surface. Exp Eye Res. 1997;64:423-30. 48.
48. Boyle DL, Takemoto L. EM immunolocalization of α-crystallins: Association with the plasma membrane from normal and cataractous human lenses. Cur Eye Res. 1996;15: 577-82.
49. Friedrich MG, Truscott RJW. Membrane association of proteins in the aging human lens: Profound changes take place in the fifth decade of life. Invest Ophthalmol Vis Sci. 2009;50:4786-93.
50. Friedrich MG, Truscott RJW. Large-scale binding of α-crystallin to cell membranes of aged normal human lenses: A phenomenon that can be induced by mild thermal stress. Invest Ophthalmol Vis Sci. 2010;51:5145-52.
51. Grami V, Marrero Y, Huang L, Tang D, Yappert MC, Borchman D. α-Crystallin binding in vitro to lipids from clear human lenses. Exp Eye Res. 2005;81:138-146.
52. Zhang WZ, Augusteyn RC. On the interaction of alpha-crystallin with membranes. Curr Eye Res. 1994;13:225-30.
53. Cenedella RJ, Chandrekher G. High capacity binding of alpha crystallins to various bovine lens membrane preparations. Curr Eye Res. 1993;11:1025-1038.
54. Mulders JWM, E Wojcik, H Blomendal. WW De Jong, Loss of high-affinity membrane binding of bovine nuclear α-crystallin. Exp Eye Res, 1989;49:149-52.
55. Cobb BA, Petrash JM, Structural and Functional Changes in the αA-Crystallin R116C Mutant in Hereditary Cataracts, Biochemistry, 2000, 39: 15791-15798.
56. Andley UP. αA-crystallin R49Cneomutation influences the architecture of lens fiber cell membranes and causes posterior and nuclear cataracts in mice. BMC Ophthalmology. 2009;9:1-11.
57. Watkins EB, Miller CE, Majewski J, Kuhl TL. Membrane texture induced by specific protein binding and receptor clustering: active roles for lipids in cellular function. Proc Nat Acad Sci (USA). 2011;108:6975-6980.
58. Hughes J, Deeley J, Blanksby SJ, Leisch F, Ellis S, Truscott RJW, Mitchell T. Instability of the cellular lipidome with age. AGE. 2012;34:935-47.

59. Huang L, Grami V, Marrero Y, Tang D, Yappert MC, Rasi V, Bourchman D. Human lens phospholipid changes with age and cataract. Invest Ophthalmol Vis Sci. 2005;46*:* 1682-89.

Figures

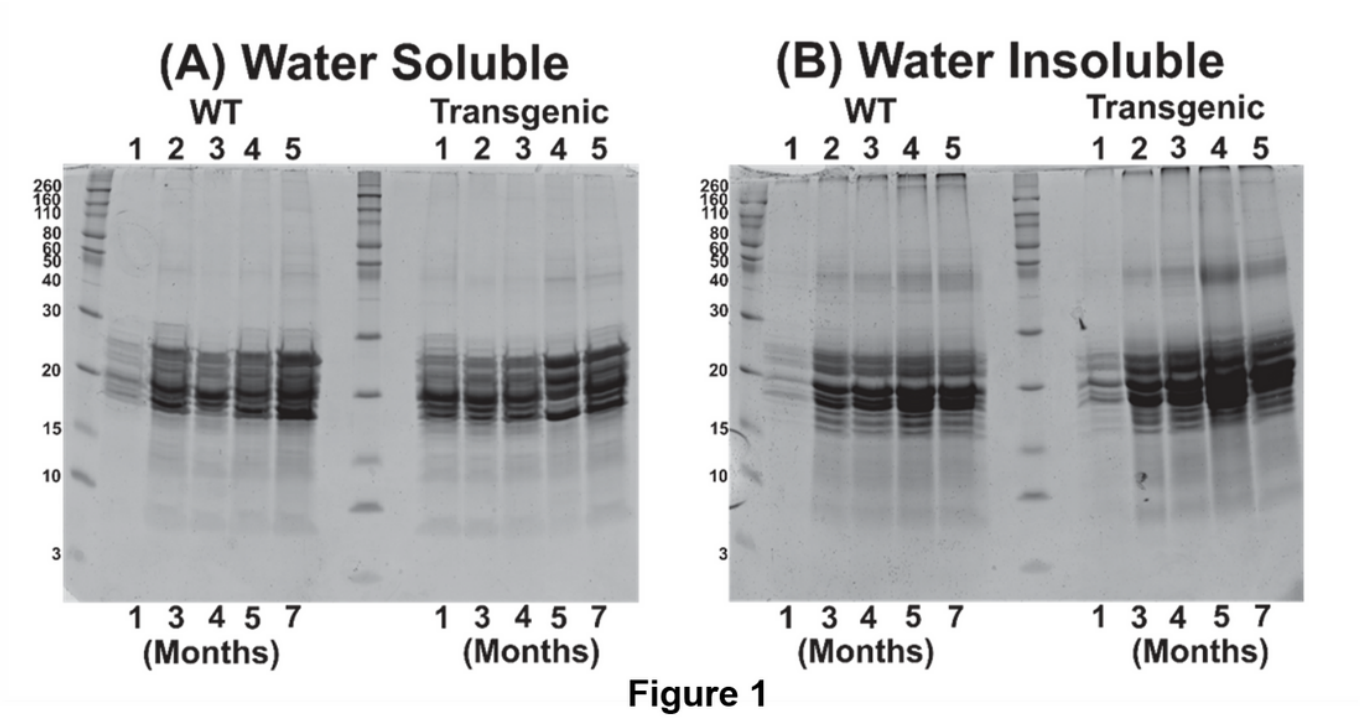

Figure 1

Table 1: Age- related changes in protein distribution in water soluble and water insoluble fractions in lenses of WT and αAN101D mice.

Age	$CRYαA_{WT}$ (mg)		$CRYαA_{N101D}$ (mg)		Percent Insoluble of total protein	
(Months)	WS	WI	WS	WI	WT	N101D
1	0.96	0.108	1.07	0.57	10.1	34.7
3	1.8	1.14	1.16	0.68	38.7	36.9
4	1.43	1.27	1.47	2	47.03	54.05
5	1.69	1.15	1.5	2.2	40.5	59.4
7	1.74	1.9	1.74	2.2	52.1	55.8

Figure 1

SDS-PAGE analysis of WS- and WI-proteins from lenses of CRYαAWT- and CRYαAN101D mice at different ages. (A). Coomassie blue stained gel of WS protein from both WT and Transgenic mice at different ages as indicated at the bottom of the gel (months). And the numbers 1-5 at the top of the gel indicate lanes. (B) Coomassie blue stained gel of WI protein from both WT and Transgenic mice at different ages as indicated at the bottom of the gel (months).). Note that a greater insolubilization and aggregated proteins (Mr >30 kDa) were seen in WI-proteins of lenses of 4-month and older CRYαAN101Dmice compared to age-matched lenses from CRYαAWT mice. The table 1. shows quantification of protein levels in the WS- and WI-protein fractions of lenses of different ages from CRYαAN101D and CRYαAWT mice. Gel images are not cropped.

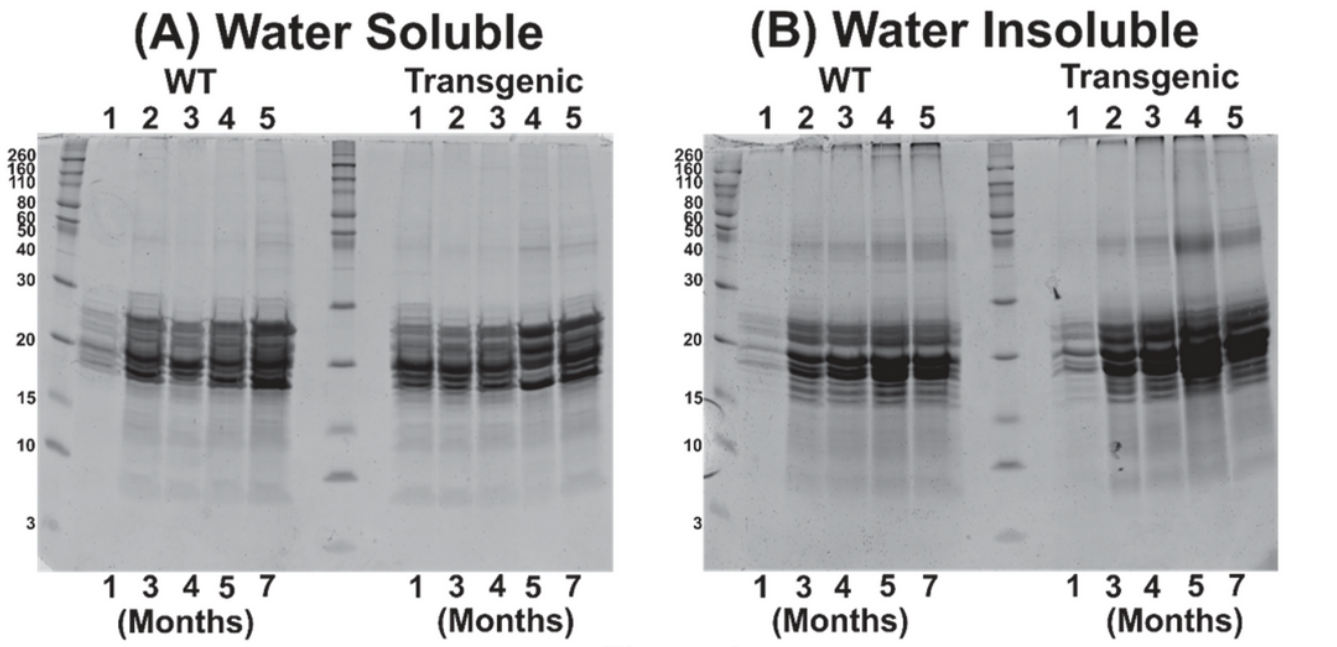

Figure 1

Table 1: Age- related changes in protein distribution in water soluble and water insoluble fractions in lenses of WT and αAN101D mice.

Age	$CRY\alpha A_{WT}$ (mg)		$CRY\alpha A_{N101D}$ (mg)		Percent Insoluble of total protein	
(Months)	WS	WI	WS	WI	WT	N101D
1	0.96	0.108	1.07	0.57	10.1	34.7
3	1.8	1.14	1.16	0.68	38.7	36.9
4	1.43	1.27	1.47	2	47.03	54.05
5	1.69	1.15	1.5	2.2	40.5	59.4
7	1.74	1.9	1.74	2.2	52.1	55.8

Figure 1

SDS-PAGE analysis of WS- and WI-proteins from lenses of CRYαAWT- and CRYαAN101D mice at different ages. (A). Coomassie blue stained gel of WS protein from both WT and Transgenic mice at different ages as indicated at the bottom of the gel (months). And the numbers 1-5 at the top of the gel indicate lanes. (B) Coomassie blue stained gel of WI protein from both WT and Transgenic mice at different ages as indicated at the bottom of the gel (months).). Note that a greater insolubilization and aggregated proteins (Mr >30 kDa) were seen in WI-proteins of lenses of 4-month and older CRYαAN101Dmice compared to age-matched lenses from CRYαAWT mice. The table 1. shows quantification of protein levels in the WS- and WI-protein fractions of lenses of different ages from CRYαAN101D and CRYαAWT mice. Gel images are not cropped.

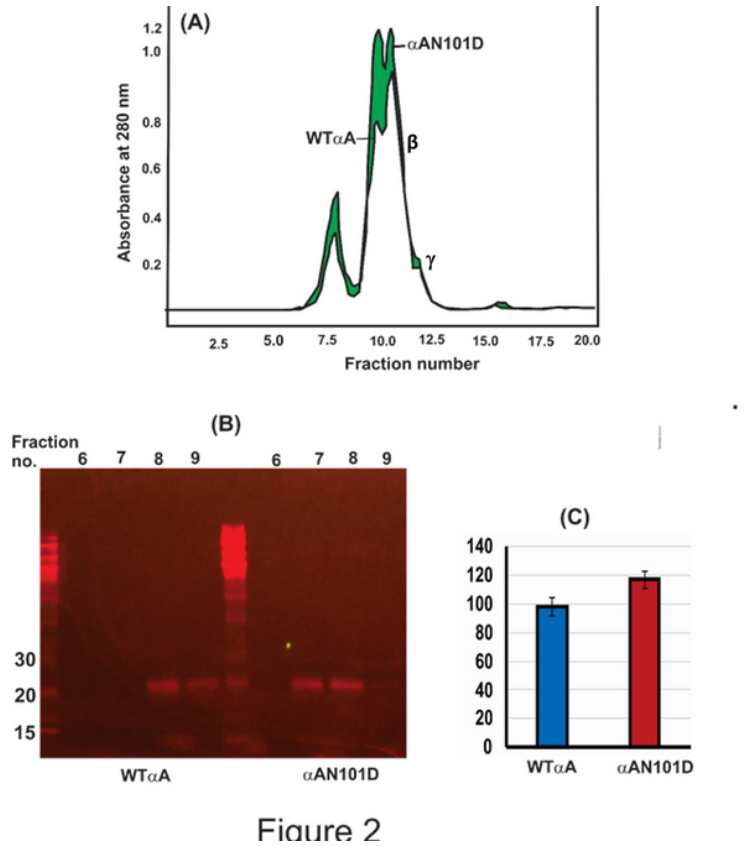

Figure 2

Figure 2

Size-exclusion HPLC (using a G-4000PWXL column) and SDS-PAGE analysis of WS-HMW proteins eluted in the void volume. (A) HPLC-protein elution profiles at 280 nm of WS-proteins from lenses of 5-month-old CRYαAN101D - and CRYαAWT mice. The green region shows the difference in the A280 profiles of WS-proteins from the two type of lenses. (B) Western blot analysis of the void volume peaks (constituted by the fraction no. 6 to 9 in [A]) following HPLC separation of WS-proteins from lenses of CRYαAN101D - and CRYαAWT mice. Note that in the CRYαAWT lenses, the αA-immunoreactive bands were in fractions no. 8 and 9 whereas it were in fraction no. 7 and 8 in CRYαAN101D lenses, suggesting a higher Mr of HMW proteins in the latter. (C) Quantification of the Western Blot using Image J. Gel images are not cropped.

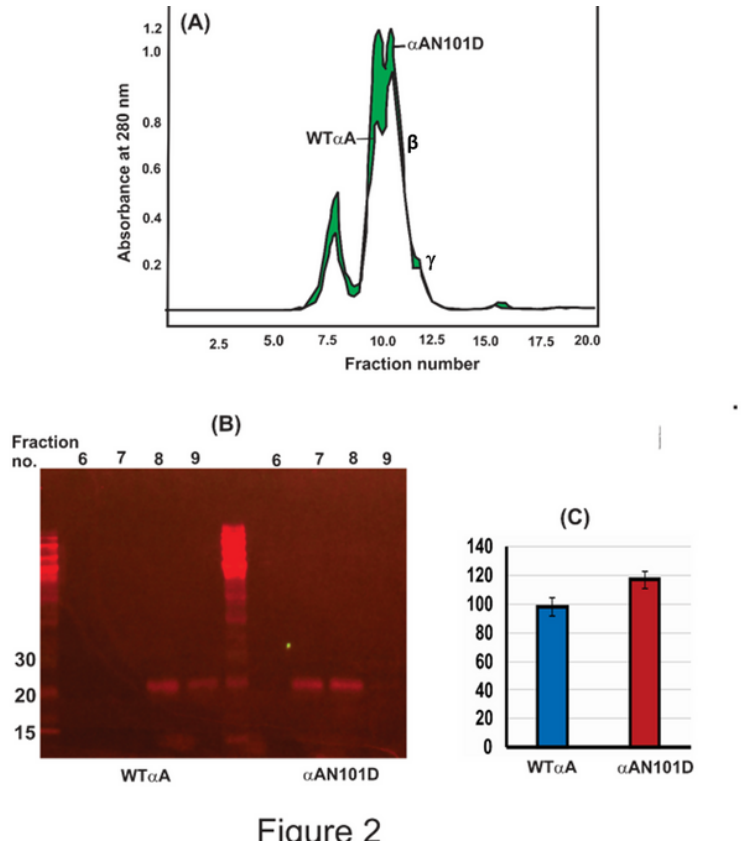

Figure 2

Figure 2

Size-exclusion HPLC (using a G-4000PWXL column) and SDS-PAGE analysis of WS-HMW proteins eluted in the void volume. (A) HPLC-protein elution profiles at 280 nm of WS-proteins from lenses of 5-month-old CRYαAN101D - and CRYαAWT mice. The green region shows the difference in the A280 profiles of WS-proteins from the two type of lenses. (B) Western blot analysis of the void volume peaks (constituted by the fraction no. 6 to 9 in [A]) following HPLC separation of WS-proteins from lenses of CRYαAN101D - and CRYαAWT mice. Note that in the CRYαAWT lenses, the αA-immunoreactive bands were in fractions no. 8 and 9 whereas it were in fraction no. 7 and 8 in CRYαAN101D lenses, suggesting a higher Mr of HMW proteins in the latter. (C) Quantification of the Western Blot using Image J. Gel images are not cropped.

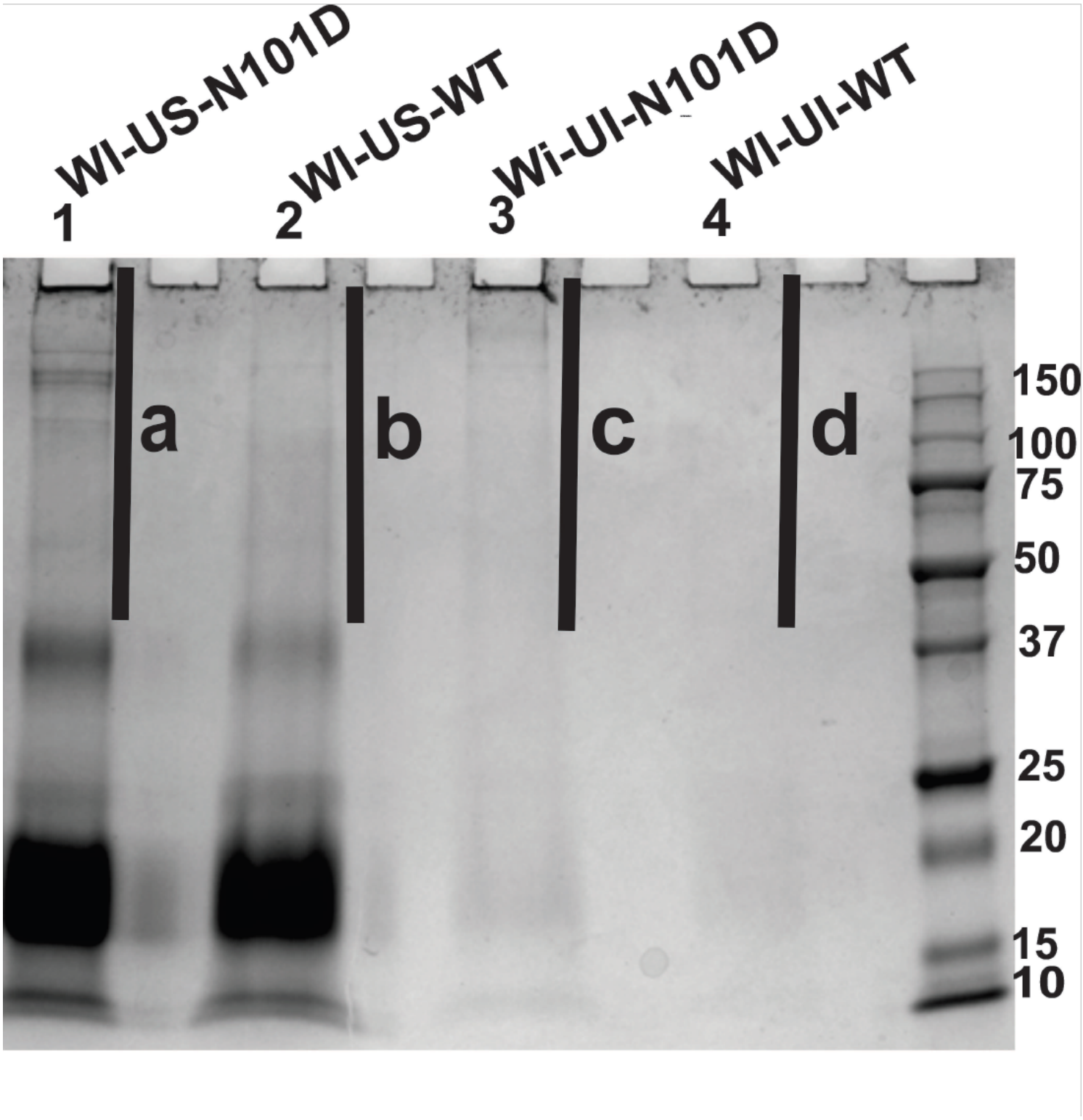

Figure 3

SDS-PAGE analysis of WI-US- and WI-UI-protein fractions of 5-month-old lenses from CRYαAN101D and CRYαAWT mice. To normalize the protein analyses, the protein fractions were isolated under identical conditions and with identical buffer volumes. Equal volumes of protein fractions from lenses of two types of mice were used during the analysis. The four fractions numbers as 1 to 4 (containing total proteins in WI-US- and WI-UI-fractions) and four fractions numbered as a to d (containing aggregated

proteins with Mr >30 kDa) were analyzed by mass-spectrometric methods, and the results are shown in supplemental Tables 1 to 4. Gel images are not cropped.

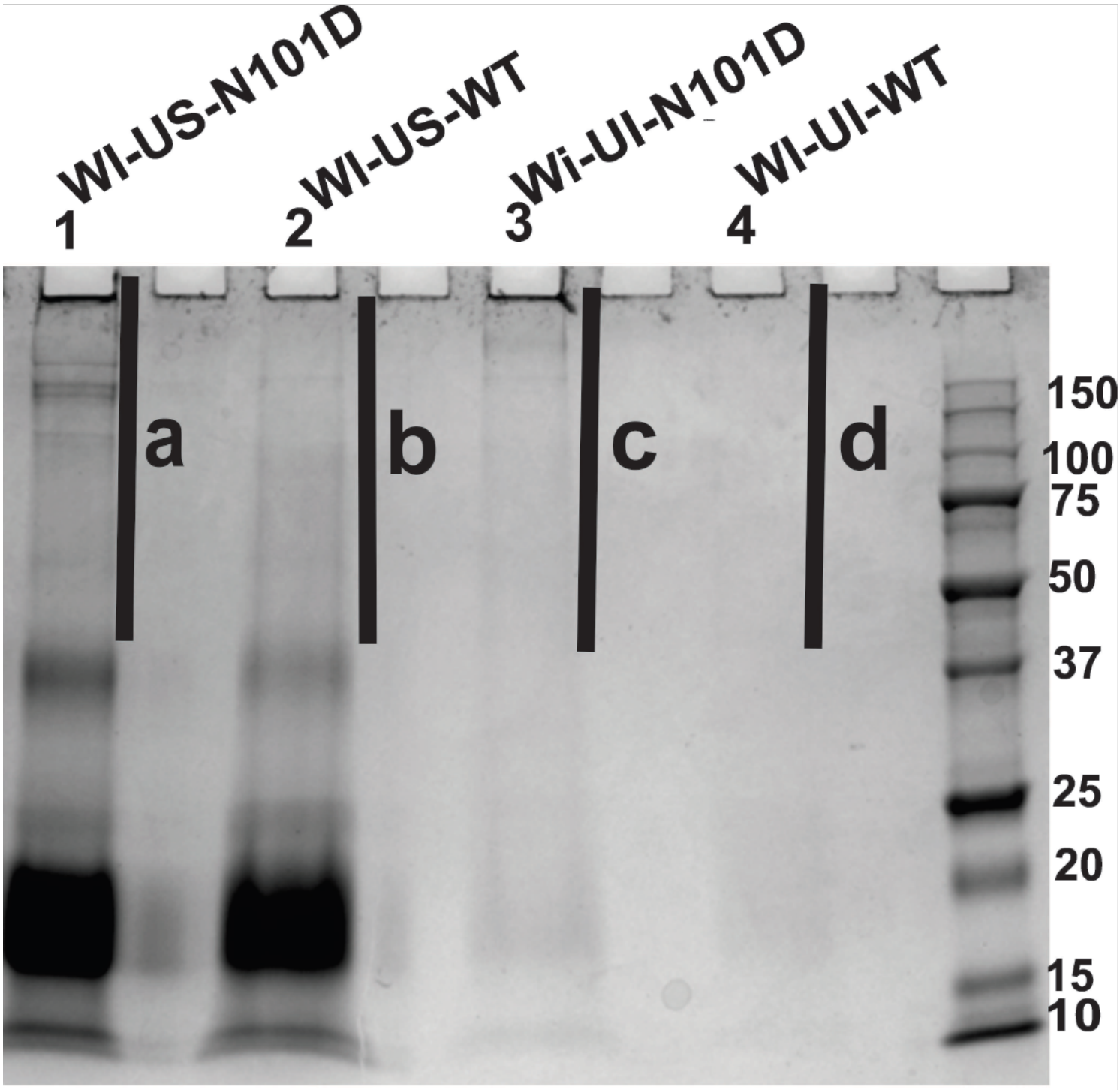

Figure 3

SDS-PAGE analysis of WI-US- and WI-UI-protein fractions of 5-month-old lenses from CRYαAN101D and CRYαAWT mice. To normalize the protein analyses, the protein fractions were isolated under identical conditions and with identical buffer volumes. Equal volumes of protein fractions from lenses of two

types of mice were used during the analysis. The four fractions numbers as 1 to 4 (containing total proteins in WI-US- and WI-UI-fractions) and four fractions numbered as a to d (containing aggregated proteins with Mr >30 kDa) were analyzed by mass-spectrometric methods, and the results are shown in supplemental Tables 1 to 4. Gel images are not cropped.

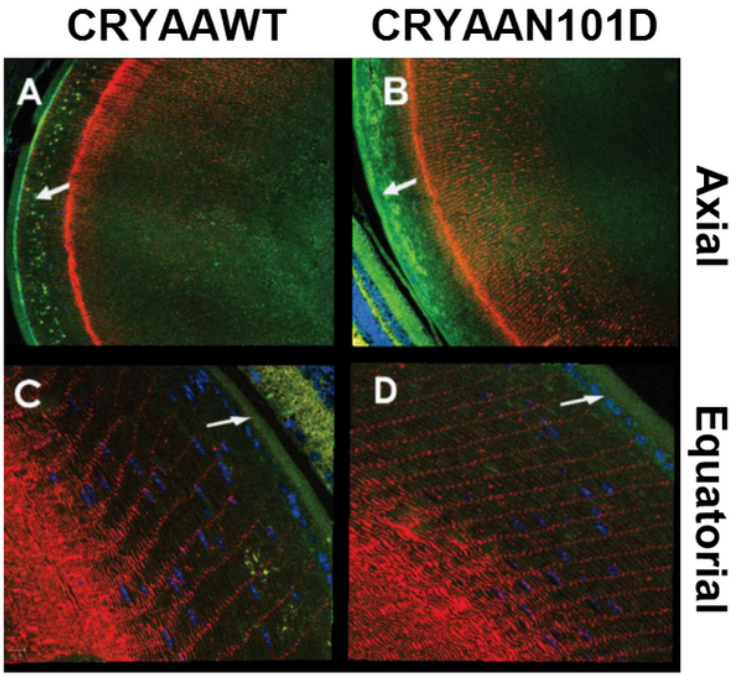

Figure 4

Figure 4

(A) Confocal-immunohistochemical analysis of 5-month old lenses from CRYαAN101D and CRYαAWT mice by using anti-His monoclonal (green, for αA detection)- and polyclonal anti-aquaporin 0 (red, for membrane detection)-antibodies. A and B: The axial sections at 10X magnification showed an irregular deposition of His-tagged αA (Green) in the lens outer cortex of CRYαAN101D mice (in B, shown by an arrow) relative to CRYαAWT mice (in A, shown by an arrow). The equatorial sections (at 40X magnification) show a greater deposit of green fluorescence in the outer cortex of CRYαAN101D lens relative to CRYαAWT (shown by arrows in Figure 4C and D).

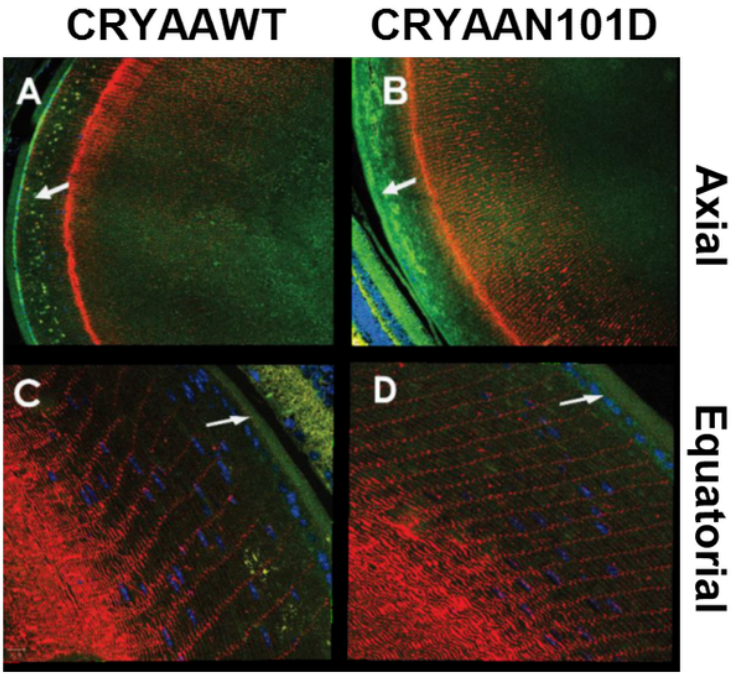

Figure 4

Figure 4

(A) Confocal-immunohistochemical analysis of 5-month old lenses from CRYαAN101D and CRYαAWT mice by using anti-His monoclonal (green, for αA detection)- and polyclonal anti-aquaporin 0 (red, for membrane detection)-antibodies. A and B: The axial sections at 10X magnification showed an irregular deposition of His-tagged αA (Green) in the lens outer cortex of CRYαAN101D mice (in B, shown by an arrow) relative to CRYαAWT mice (in A, shown by an arrow). The equatorial sections (at 40X magnification) show a greater deposit of green fluorescence in the outer cortex of CRYαAN101D lens relative to CRYαAWT (shown by arrows in Figure 4C and D).

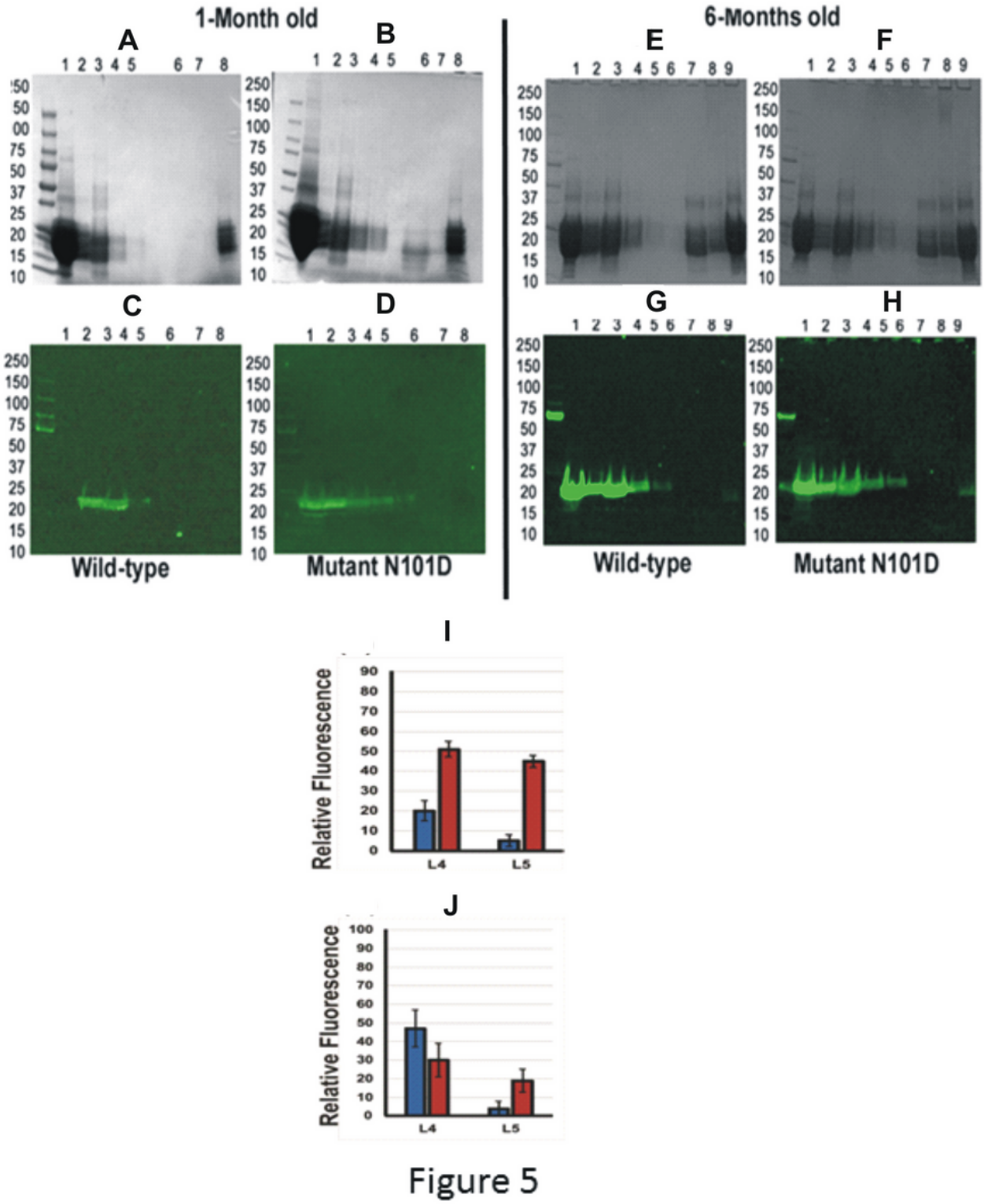

Figure 5

Figure 5

Relative Membrane-Association of WTαA- and αAN101D in Lenses of CRYαAN101D and CRYαAWT Mice. Figures A, B, E and F: The relative levels of association of WTαA and αAN101D with the purified membrane preparations at different membrane purification steps analyzed using SDS-PAGE analysis at two different age groups (1 and 6 months) Figures C, D, G and H: Similarly the samples were analyzed by Western blot using anti-His antibody at two different age groups (1and 6 months). Additionally, in both

left and right panels, the lanes 1, 2 and 3 show the WS-protein fractions recovered after 1st, 2nd and 3rd consecutive washes in buffer B to solubilize WS-proteins, respectively. Lanes 4 and 5 represent the urea soluble-protein fractions recovered during two consecutive washes of WI-protein pellet with buffer B containing 8M urea, similarly, lanes 7 and 8 from 6-month old lenses (E and F) represent purified membrane preparation. Lane 9 of 6-month old lenses represents crude WS-homogenate. I & J: Quantification of immunoreactive bands of αA- recovered in urea-soluble fractions (Lane 4 [L4] and lane 5 [L5] represent two consecutive urea wash of WI proteins during membrane isolation from lenses of CRYαAWT and CRYαAN101Dmice as shown in Western blot analysis in Figure 5. (I) Relative levels of immunoreactive WTαA lenses (blue) and αA-N101D αA- (red) during membrane purification from 1-month old lenses. (J) Relative levels of immunoreactive WTαA lenses (blue) and αAN101D αA- (red) during membrane purification from 6-months old lenses. Note that relatively higher levels of αAN101D than WTαA was associated with purified membranes in lanes 4 (in 1-month old) and lane 5 (in both 1- and 6-month-old) of the two types of lenses. Gel images are not cropped.

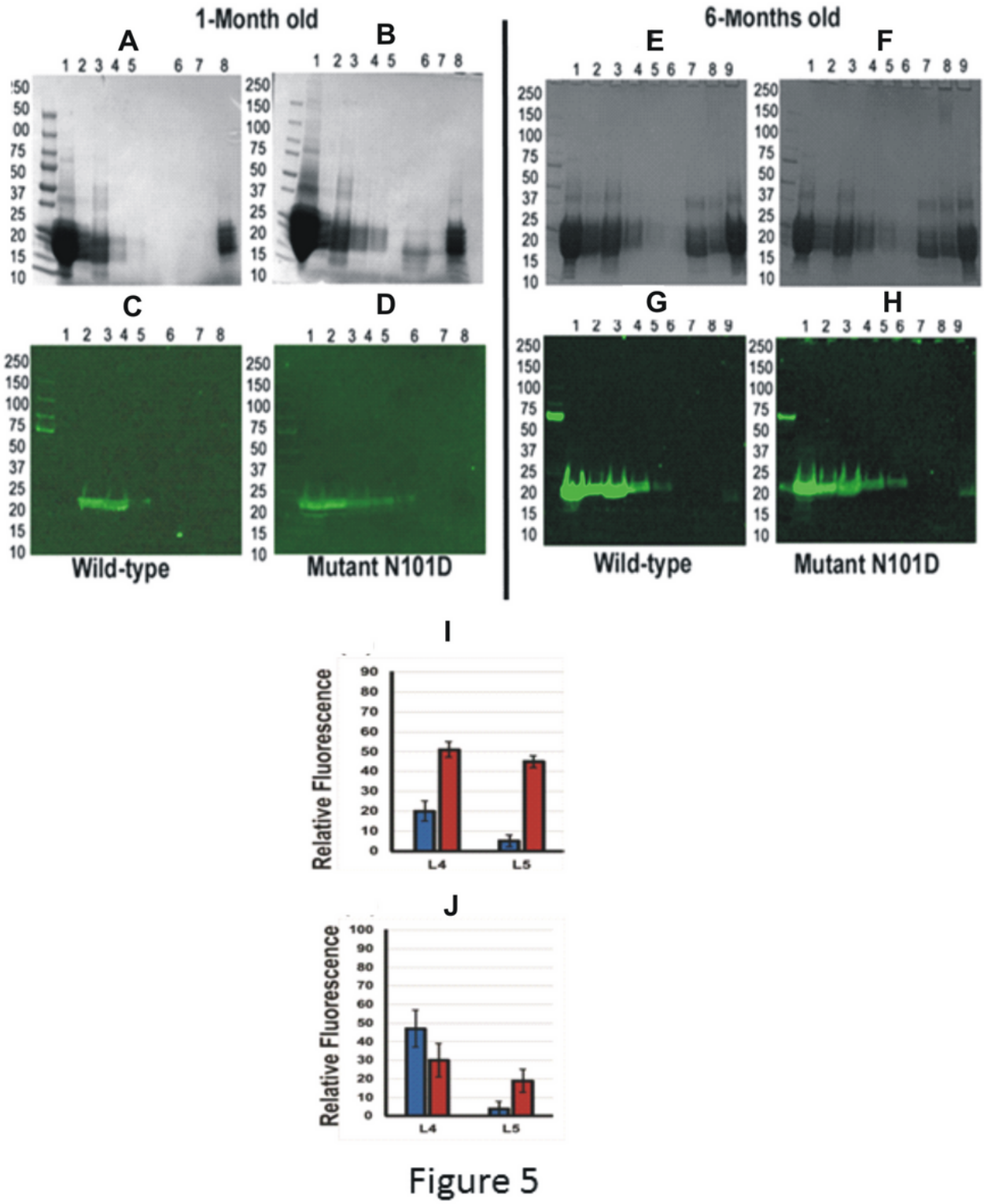

Figure 5

Figure 5

Relative Membrane-Association of WTαA- and αAN101D in Lenses of CRYαAN101D and CRYαAWT Mice. Figures A, B, E and F: The relative levels of association of WTαA and αAN101D with the purified membrane preparations at different membrane purification steps analyzed using SDS-PAGE analysis at two different age groups (1 and 6 months) Figures C, D, G and H: Similarly the samples were analyzed by Western blot using anti-His antibody at two different age groups (1and 6 months). Additionally, in both

left and right panels, the lanes 1, 2 and 3 show the WS-protein fractions recovered after 1st, 2nd and 3rd consecutive washes in buffer B to solubilize WS-proteins, respectively. Lanes 4 and 5 represent the urea soluble-protein fractions recovered during two consecutive washes of WI-protein pellet with buffer B containing 8M urea, similarly, lanes 7 and 8 from 6-month old lenses (E and F) represent purified membrane preparation. Lane 9 of 6-month old lenses represents crude WS-homogenate. I & J: Quantification of immunoreactive bands of αA- recovered in urea-soluble fractions (Lane 4 [L4] and lane 5 [L5] represent two consecutive urea wash of WI proteins during membrane isolation from lenses of CRYαAWT and CRYαAN101Dmice as shown in Western blot analysis in Figure 5. (I) Relative levels of immunoreactive WTαA lenses (blue) and αA-N101D αA- (red) during membrane purification from 1-month old lenses. (J) Relative levels of immunoreactive WTαA lenses (blue) and αAN101D αA- (red) during membrane purification from 6-months old lenses. Note that relatively higher levels of αAN101D than WTαA was associated with purified membranes in lanes 4 (in 1-month old) and lane 5 (in both 1- and 6-month-old) of the two types of lenses. Gel images are not cropped.

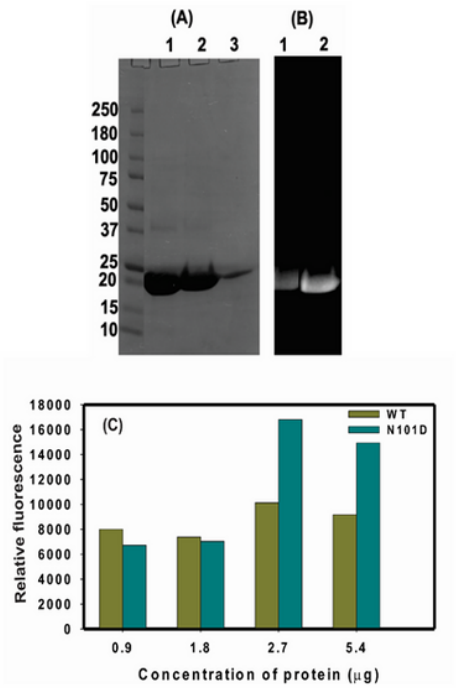

Figure 6

Figure 6

Relative in vitro binding of recombinant αAN101D and WTαA proteins to lens membrane. (A) The recombinant WT αA- and αA-N101D proteins were labeled with Alexa 350, purified by a size-exclusion HPLC column and analyzed by SDS-PAGE. Lane 1: Coomassie blue-stained WTαA, lane 2: αAN101D mutant protein, and lane 3: purified lens membrane from non-transgenic C57 mice. (B) Images of labeled αAN101D and WTαA proteins. Lane 1: Alexa 350-labeled WT αA, and lane 2: αAN101D protein. (C) Binding of a WT αA, and αAN101D with purified lens membrane (2.5 mg protein; isolated from 1- to 3-month old non-transgenic C57 mice). During the binding assay, the protein mixtures were incubated with

increasing but identical concentrations of either Alexa-labelled WTαA- or αA-N101D at 37oC for 6 h, centrifuged at 14,000Xg and the supernatant and pellet (membrane fraction) recovered. After washing the membrane fraction with water and centrifugation as above, the relative fluorescence of membranes incubated with WT αA- and αA-N101D mutant proteins was determined. The values reported are the average of triplicate assays.

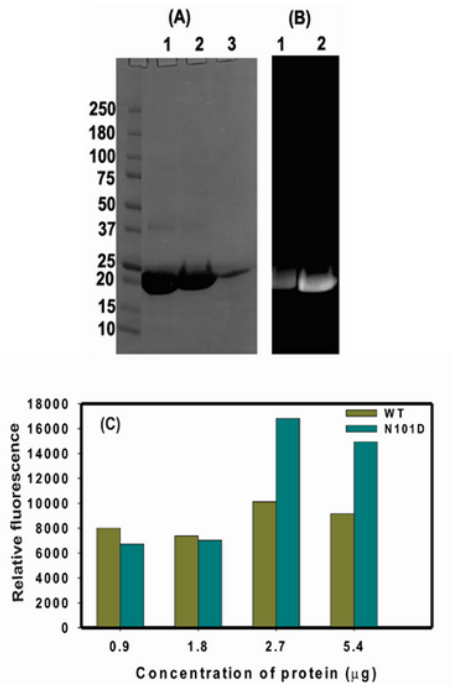

Figure 6

Figure 6

Relative in vitro binding of recombinant αAN101D and WTαA proteins to lens membrane. (A) The recombinant WT αA- and αA-N101D proteins were labeled with Alexa 350, purified by a size-exclusion HPLC column and analyzed by SDS-PAGE. Lane 1: Coomassie blue-stained WTαA, lane 2: αAN101D mutant protein, and lane 3: purified lens membrane from non-transgenic C57 mice. (B) Images of labeled αAN101D and WTαA proteins. Lane 1: Alexa 350-labeled WT αA, and lane 2: αAN101D protein. (C) Binding of a WT αA, and αAN101D with purified lens membrane (2.5 mg protein; isolated from 1- to 3-month old non-transgenic C57 mice). During the binding assay, the protein mixtures were incubated with increasing but identical concentrations of either Alexa-labelled WTαA- or αA-N101D at 37oC for 6 h, centrifuged at 14,000Xg and the supernatant and pellet (membrane fraction) recovered. After washing the membrane fraction with water and centrifugation as above, the relative fluorescence of membranes incubated with WT αA- and αA-N101D mutant proteins was determined. The values reported are the average of triplicate assays.

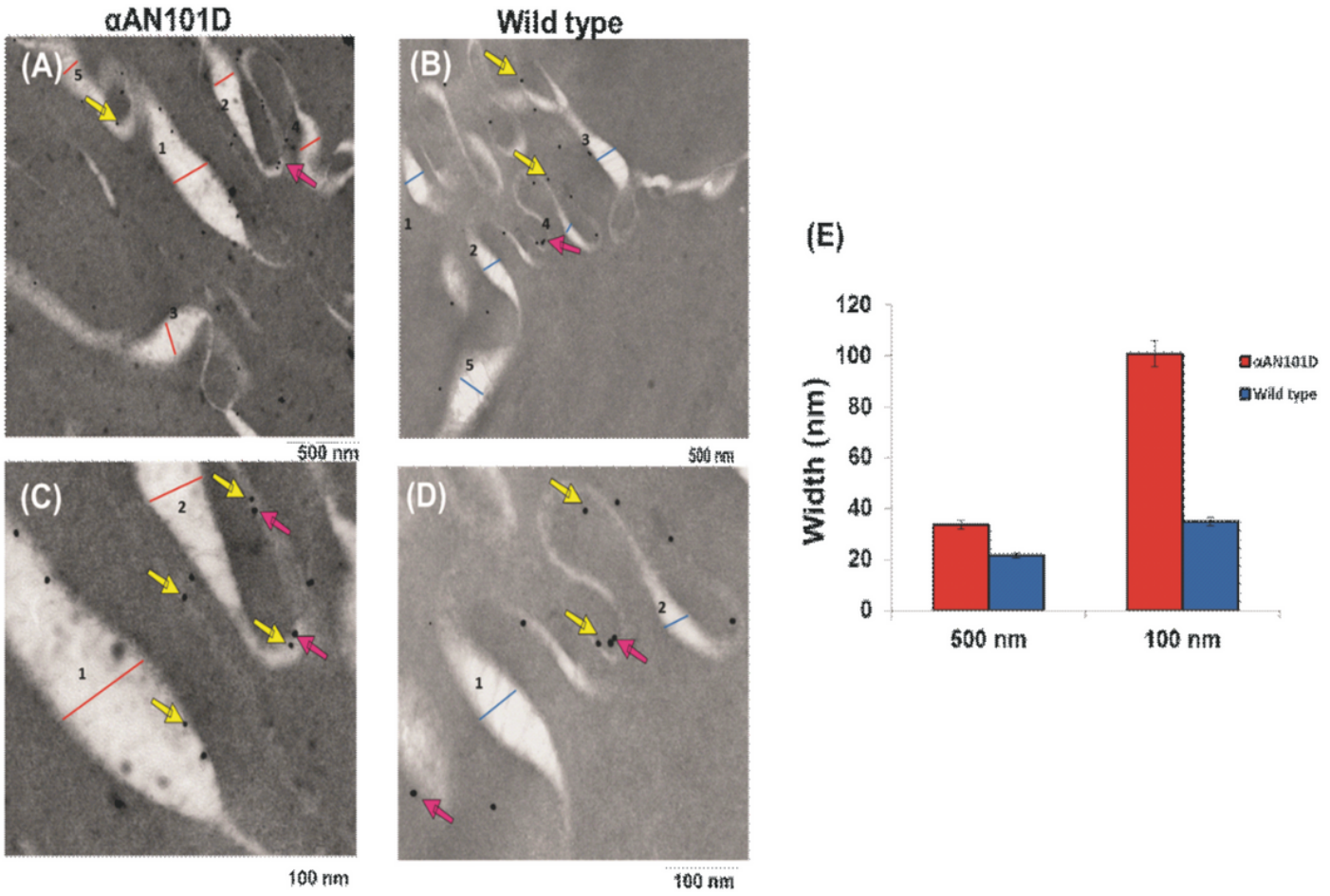

Figure 7

Immunogold-labeling to determine relative localization of αA-WT and αAN101D in lens membranes of CRYαAN101D and CRYαAWT mice. (A) and (C) show membranes of lenses from CRYαAN101D (at 500 nm and 100 nm magnification respectively) and (B) and (D) from CRYαAWT (at 500 nm and 100 nm magnification respectively). The bigger particles (25 nm, red arrows) represented the aquaporin 0 whereas the smaller gold particles (10 nm, yellow arrows) represented the His-tagged αAN101D and WTαA-. As shown in the representative images in (A) to (D), both 10 nm and the 25 nm gold particles were bound to membranes. (E): Quantification of width of membranes from lenses of CRYαAN101D and CRYαAWT mice. Note that the lens membranes of CRYαAN101D mice were about 2X wider that those from CRYαAN101D mice, suggesting membrane swelling of the former lenses.

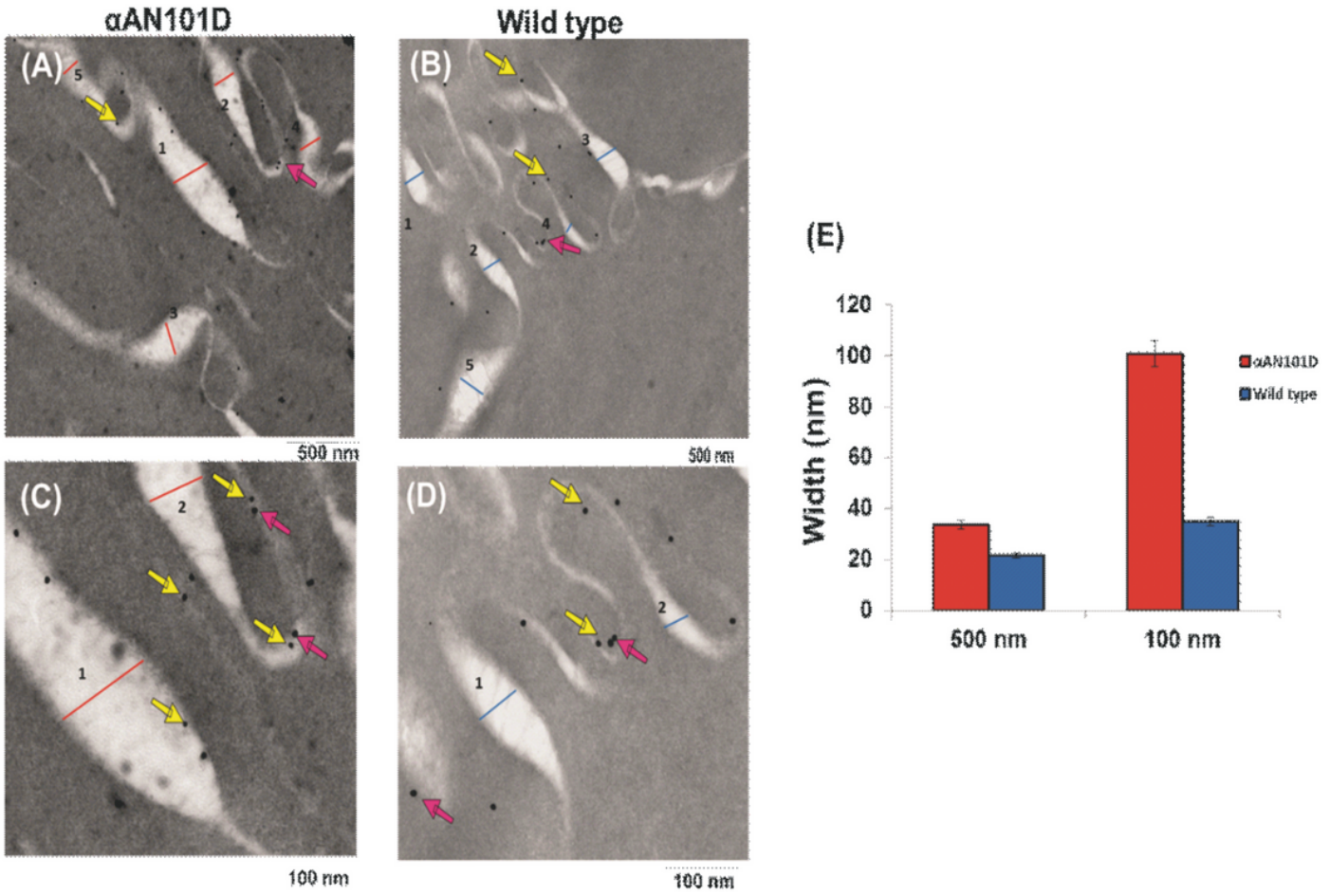

Figure 7

Immunogold-labeling to determine relative localization of αA-WT and αAN101D in lens membranes of CRYαAN101D and CRYαAWT mice. (A) and (C) show membranes of lenses from CRYαAN101D (at 500 nm and 100 nm magnification respectively) and (B) and (D) from CRYαAWT (at 500 nm and 100 nm magnification respectively). The bigger particles (25 nm, red arrows) represented the aquaporin 0 whereas the smaller gold particles (10 nm, yellow arrows) represented the His-tagged αAN101D and WTαA-. As shown in the representative images in (A) to (D), both 10 nm and the 25 nm gold particles were bound to membranes. (E): Quantification of width of membranes from lenses of CRYαAN101D and CRYαAWT mice. Note that the lens membranes of CRYαAN101D mice were about 2X wider that those from CRYαAN101D mice, suggesting membrane swelling of the former lenses.

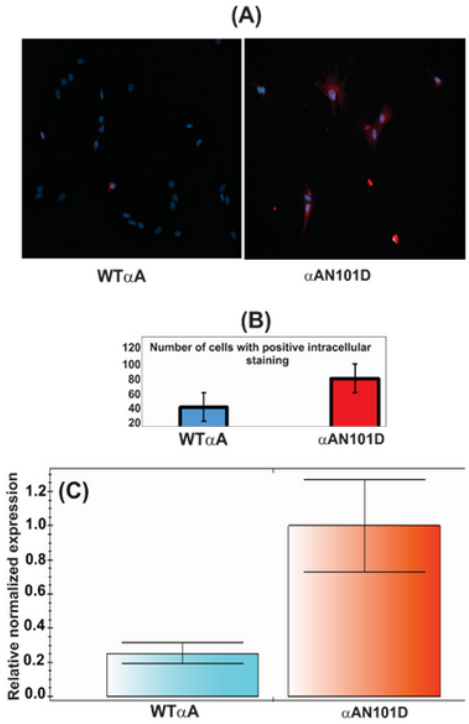

Figure 8

Figure 8

Determination of levels of intracellular Ca2+ and Na, K-ATPase mRNA in cultured epithelial cells from lenses of CRYαAN101D and CRYαAWT mice. (A) Left and right panels show intracellular Ca2+ staining following uptake from calcium orange in cells from CRYαAWT- and CRYαAN101D mice, respectively. (B) Quantification by Image J of the number of cells that showed positive intracellular Ca2+-staining following uptake from calcium orange in CRYαAWT - and CRYαAN101D cells. (C) Relative levels of Na, K-ATPase mRNA in epithelial cells from CRYαAWT- and CRYαAN101D mice as determined by the QRT-PCR method.

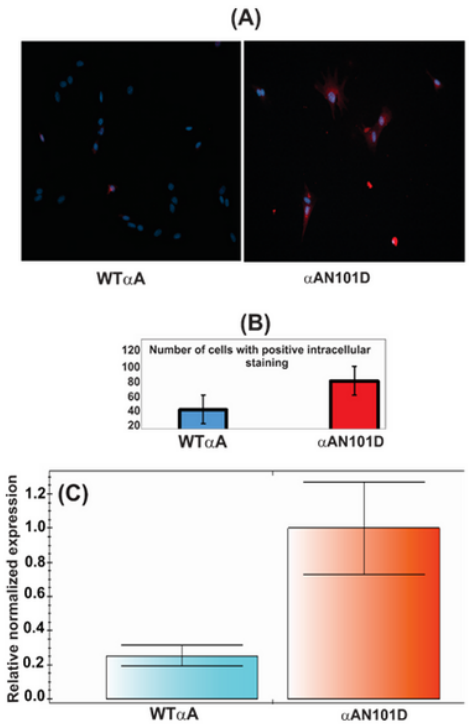

Figure 8

Figure 8

Determination of levels of intracellular Ca2+ and Na, K-ATPase mRNA in cultured epithelial cells from lenses of CRYαAN101D and CRYαAWT mice. (A) Left and right panels show intracellular Ca2+ staining following uptake from calcium orange in cells from CRYαAWT- and CRYαAN101D mice, respectively. (B) Quantification by Image J of the number of cells that showed positive intracellular Ca2+-staining following uptake from calcium orange in CRYαAWT - and CRYαAN101D cells. (C) Relative levels of Na, K-ATPase mRNA in epithelial cells from CRYαAWT- and CRYαAN101D mice as determined by the QRT-PCR method.

Supplementary Files

This is a list of supplementary files associated with this preprint. Click to download.

- NC3RsARRIVEGuidelinesChecklist.pdf
- NC3RsARRIVEGuidelinesChecklist.pdf
- SupplementalTableA.xlsx
- SupplementalTableA.xlsx
- SupplementalTableB.xlsx
- SupplementalTableB.xlsx
- SupplementalTableC.xlsx

- SupplementalTableC.xlsx
- SupplementalTableD.xlsx
- SupplementalTableD.xlsx